Chapter 4

Control Techniques for Matrix Converters

Since its first description in [1] the matrix converter has been the subject of an intensive ongoing research, and the aspect which has attracted much of the research effort has been the control techniques. For direct AC-AC matrix converters used in adjustable speed drives the ideal control technique should:

- provide independent control of the magnitude and frequency of the generated output voltages;
- give sinusoidal input currents with full control of the displacement angle;
- provide the maximum output to input voltage ratio;
- satisfy the conflicting requirements of minimum low order harmonics and minimum switching losses,
- be able to compensate the effects of unbalanced and/or distortions of the supply input voltages;
- be computationally efficient.

The control scheme originally proposed in [1], although characterized by better performance than naturally commutated cycloconverters, it had significant output voltage limitations and serious waveforms distortion.

In 1980 Venturini proposed in [2] an alternative high switching frequency control technique which was more effective than traditional control techniques, but still having a maximum output voltage equal to half of the input voltage and a restriction in the input power factor control.

In 1985 Ziogas et alia proposed in [3] and [4] a control technique that was based on a totally different approach, in which the input voltages are first "rectified" to create a fictitious DC bus and then "inverted" to assemble the output voltages at the required frequency. Computationally complicated, this control technique yielded improved waveforms and higher input voltage utilization, but still had limitations in the input-output harmonic distortion and in the input power factor control.

In 1987 Schauder patented in [5] a control technique based on a similar rectifier-inverter concept which emulates the action of a DC-link inverter, but derived on simplistic considerations

of input and output power. Experimentally proved in [6] this technique provided improved input and output waveforms along with maximum voltage transfer ratio and unity input power factor. But some limitations still remained in the input power factor control and input voltage disturbances compensation.

In 1988 Venturini and Alesina proposed in [7] an improved control algorithm that raised the maximum input-output voltage transfer ratio to 0.867, which was demonstrated to be the theoretical limit under the constraint of sinusoidal input and output waveforms, and provided for full input power factor control and compensation of input voltages unbalance and/or distortion.

In 1989 Roy and April proposed in [8] an interesting scalar control algorithm, with performance comparable to the Venturini method's apart from the input disturbance compensation capability but computationally more efficient.

In 1989 Huber and Borojevic proposed in [9] the first control technique for matrix converter based on space vector modulation. Using a space vector representation of the input and output currents and voltages, the approach of the proposed control technique resembled the rectifier-inverter concept, considering the matrix converter as a two stage transformation converter: a rectification stage which provides a constant imaginary DC-link and an inverter stage which produces the three phase target voltages. In this way a so called "indirect" space vector modulation of input currents and output voltages was carried out. An improved version of the control algorithm that allowed for input power factor control and compensation of input voltages distortion was proposed in [10] in 1991. Despite of this technique basically provides performance as good as the Venturini's technique, it adds some advantages in terms of digital implementation and better representation of the power conversion process.

In 1993 Casadei, Tani *et alia* proposed in [11] a new control method based on space vector modulation. The originality of the proposed control algorithm resides in its different approach to the matrix converter control, which does not make use of any imaginary DC-link but physically adheres to the direct power conversion process carried out by the matrix converter. The on-time durations of the permitted matrix converter switches combinations are derived under the assumption that the output voltages are directly assembled from consecutive "chops" of the input voltages. Compared to the Venturini's method and the Indirect SVM techniques, the "Direct SVM" control method provides comparable performance but yields a more physical adherence to and an immediate comprehension of the direct power conversion process. These become key features when unconventional control strategies has to be design. Last but not least, due to its compact and easy formula, the control of the input power factor and the compensation of input voltages distortion can be easily carried out without significant addition of calculations.

This chapter focuses on different matrix converter modulation strategies based on space vector modulation. By means of a simulation model the performance of these strategies have been analyzed under either balanced and sinusoidal or unbalanced and nonsinusoidal supply

voltage conditions. The numerical results have been verified by experimental tests carried out on a matrix converter prototype during a six month working period at the Institute of Energy Technology at the University of Aalborg, Denmark.

4.1 Brief introduction to the space vector representation of a three phase system

For the reader that might be not familiar to the use of space vectors for representing three phase quantities, the basic formulae and concepts are briefly recalled in this section.

For the analysis of a three phase system, the instantaneous space vector representation can be utilized according to the following transformation

$$\bar{x} = x_d + j\,x_q = \frac{2}{3}\left(x_a + \bar{a}\,x_b + \bar{a}^2\,x_c \right) \tag{4.1}$$

where $\bar{a} = e^{j\frac{2\pi}{3}}$.

With the condition $x_a + x_b + x_c = 0$, the inverse transformation is

$$x_a = \bar{x} \cdot 1, \qquad x_b = \bar{x} \cdot \bar{a}, \qquad x_c = \bar{x} \cdot \bar{a}^2 \tag{4.2}$$

where $(\cdot)$ denotes the scalar product.

If the three phase system is supposed to be periodical with period $T = 2p/w$, the space vector components are periodical too and can be decomposed in the complex Fourier series [12]

$$\bar{x}(t) = \sum_{k=-\infty}^{+\infty} \bar{X}_k\, e^{j\,k\,\omega t} \tag{4.3}$$

where

$$\bar{X}_k = \frac{1}{T}\int_0^T \bar{x}(t)\, e^{-j\,k\,\omega t}\, dt \qquad k = 0, \pm 1, \pm 2, \ldots, \infty \tag{4.4}$$

represents the time phasor of the kth harmonic component.

Indicating by $\bar{X}_p$ the positive sequence fundamental component and by $\bar{X}_n^*$ the negative sequence fundamental component, the equation (4.4) written for k = ±1 gives

$$\begin{aligned} \bar{X}_1 &= \bar{X}_p \\ \bar{X}_{-1} &= \bar{X}_n^* \end{aligned} \tag{4.5}$$

For a sinusoidal and balanced three phase system the relevant space vector has constant magnitude and constant rotating speed, which is equal to the angular frequency w of the system. The corresponding equations are given hereinafter.

$$\left.\begin{aligned} x_1 &= X_{max}\cos(\omega t + \vartheta_i) \\ x_2 &= X_{max}\cos\left(\omega t + \vartheta_i - \frac{2\pi}{3}\right) \\ x_3 &= X_{max}\cos\left(\omega t + \vartheta_i - \frac{4\pi}{3}\right) \end{aligned}\right\} \qquad (4.6)$$

where q_i is the phase angle at the instant t = 0. Substituting expressions (4.6) in (4.1) the following space vector expression can be derived

$$\bar{x} = X_{max}\, e^{\,j\vartheta_i}\, e^{\,j\omega t} = \overline{X}\, e^{\,j\omega t} \qquad (4.7)$$

As it is shown by Fig.4.1.a, the trajectory described by this space vector in the Gauss plane is a circumference.

In the case the three phase system is sinusoidal but unbalanced, the related space vector consists of the positive and negative sequence fundamental components. Therefore, accordingly to (4.5) the space vector $\bar{x}$ can be written as

$$\bar{x} = \overline{X}_1\, e^{\,j\omega t} + \overline{X}_{-1}\, e^{-j\omega t} \qquad (4.8)$$

Due to the presence of the negative sequence component, both magnitude and rotating speed of the space vector vary in time. In this case the locus described by the space vector $\bar{x}$ is an ellipse, as shown in Fig.4.1.b.

Likewise, if the three phase system is nonsinusoidal and balanced, the space vector consists of a positive sequence fundamental component plus other components representing the distorting harmonic components. As before, magnitude and rotating speed of the system space vector are not constant in time. In Fig.4.1.c it is shown the locus described by the following space vector

$$\bar{x} = \overline{X}_1\, e^{\,j\omega t} + \overline{X}_{-5}\, e^{-j5\omega t} \qquad (4.9)$$

where $\overline{X}_{-5}\, e^{-j5\omega t}$ is the vector component correspondent to a 5^{th} negative harmonic component.

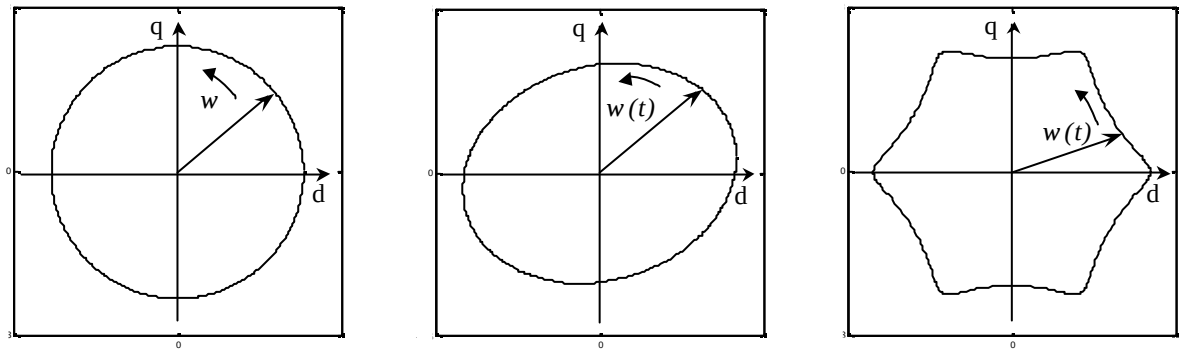

a) b) c)

Fig.4.1. Space vector loci for different three phase systems.
a) Sinusoidal and balanced. b) Sinusoidal and unbalanced. c) Non-sinusoidal and balanced.

4.2 Space vector approach for Matrix Converter

As aforementioned the three-phase to three-phase matrix converter consists of 9 bi-directional switches through which it connects two independent three phase systems.

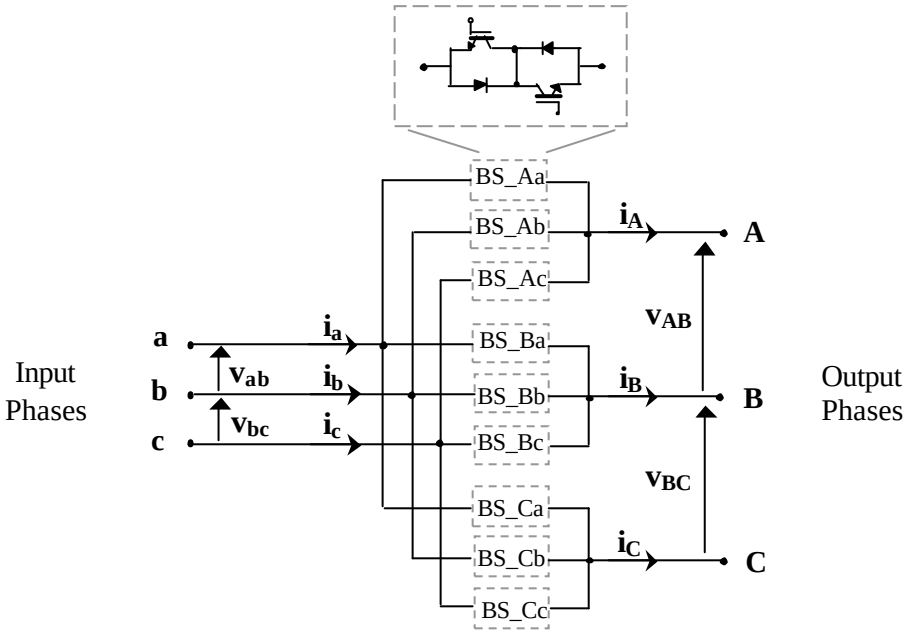

Fig.4.2 Three-phase to three-phase matrix converter.

With reference to the matrix converter and the relevant symbols shown in Fig.4.2 and accordingly to equation (4.1), it is possible to define the following space vectors:

$$\bar{v}_i = \frac{2}{3}(v_{ab} + \bar{a}\, v_{bc} + \bar{a}^2 v_{ca}) = v_i(t)\, e^{j\alpha_i(t)} \tag{4.10}$$

$$\bar{v}_o = \frac{2}{3}(v_{AB} + \bar{a}\, v_{BC} + \bar{a}^2 v_{CA}) = v_o(t)\, e^{j\alpha_o(t)} \tag{4.11}$$

$$\bar{i}_i = \frac{2}{3}(i_a + \bar{a}\, i_b + \bar{a}^2 i_c) = i_i(t)\, e^{j\beta_i(t)} \tag{4.12}$$

$$\bar{i}_o = \frac{2}{3}(i_A + \bar{a}\, i_B + \bar{a}^2 i_C) = i_o(t)\, e^{j\beta_o(t)} \tag{4.13}$$

where $v_i(t)$, $v_o(t)$, $i_i(t)$ and $i_o(t)$ are the time dependent magnitudes of the space vectors while $a_i(t)$, $a_o(t)$, $b_i(t)$ and $b_o(t)$ are the corresponding time dependent phase angles.

Now, these four space vectors can be defined for any matrix converter switches configuration (in the following also simply configuration). But not all the possible configurations that a matrix converter can assume can be usefully employed. Taking into account that the

converter is generally supplied at the input by a voltage source and it feeds at the output an inductive load, two rules have to be always respected:

i) the input phases should never be short-circuited;

ii) the output current should never be interrupted.

Under these constraints it can be verified that in a three-phase to three-phase matrix converter only 27 different switches configurations are permitted. These 27 switches configurations are listed in Table I. Each configuration is identified by a number and by a three-letter code. The three letters describe which output phase is connected to which input phase accordingly to the schematic representation of Fig.4.3.

For instance, the configuration named **aca** refers to the matrix state where output phase **A** is connected to input phase **a**, output phase **B** is connected to input phase **c** and output phase **C** is connected to input phase **a**.

In Table I, for each configuration the relevant output line-to-line voltages are given as function of the input line-to-line voltages, which are impressed by the grid, as well as the input converter currents are expressed as function of the output line currents, which are impressed by the load.

Accordingly to the corresponding output line-to-line voltage and input current space vectors, these matrix converter configurations are classified as “active”, “zero” and “synchronous” configurations.

The active configurations are 18 and numbered from ±1, ±2,.., ±9 in Table I. They determine six prefixed positions of the output line-to-line voltage space vector $\bar{v}_o$ which are not dependent on the input line-to-line voltage space vector phase angle $a_i(t)$ and six prefixed positions of the input current space vector $\bar{i}_i$ which are not dependent on the output line current space vector angle $b_o(t)$. The magnitude of the space vectors $\bar{v}_o$ and $\bar{i}_i$ is variable and depends on the instantaneous values of the input line-to-line voltages and output line currents respectively. The active configurations have also the common feature of two output lines (or phases) connected to the same input line (or phase) as it can be seen in Table I, by the second column starting from the left hand side.

The zero configuration are 3. In zero configurations the three output lines are connected to the same input phase, so that they determine zero output line-to-line voltage and input current space vectors.

The synchronous configurations are 6 and not numbered in Table I. These configurations determine output line-to-line voltage space vector $\bar{v}_o$ having a phase angle $a_o(t)$ which is dependent on the input line-to-line voltage space vector phase angle $a_i(t)$. Likewise, the input current space vector $\bar{i}_i$ has a phase angle $b_i(t)$ which is related to the output line current space vector phase angle $b_o(t)$.

The magnitude of the space vectors $\bar{v}_o$ and $\bar{i}_i$ is constant and equal to the magnitude of the input line-to-line voltage and output line current space vectors respectively.

Table I.
List of the 27 possible matrix converter switches configurations.

Switches Configurations	A	B	C	v_{AB}	v_{BC}	v_{CA}	i_a	i_b	i_c	v_o	a_o	i_i	b_i
+1	a	b	b	v_{ab}	0	$-v_{ab}$	i_A	$-i_A$	0	$2/\sqrt{3}\, v_{ab}$	p/6	$2/\sqrt{3}\, i_A$	-p/6
-1	b	a	a	$-v_{ab}$	0	v_{ab}	$-i_A$	i_A	0	$-2/\sqrt{3}\, v_{ab}$	p/6	$-2/\sqrt{3}\, i_A$	-p/6
+2	b	c	c	v_{bc}	0	$-v_{bc}$	0	i_A	$-i_A$	$2/\sqrt{3}\, v_{bc}$	p/6	$2/\sqrt{3}\, i_A$	p/2
-2	c	b	b	$-v_{bc}$	0	v_{bc}	0	$-i_A$	i_A	$-2/\sqrt{3}\, v_{bc}$	p/6	$-2/\sqrt{3}\, i_A$	p/2
+3	c	a	a	v_{ca}	0	$-v_{ca}$	$-i_A$	0	i_A	$2/\sqrt{3}\, v_{ca}$	p/6	$2/\sqrt{3}\, i_A$	7p/6
-3	a	c	c	$-v_{ca}$	0	v_{ca}	i_A	0	$-i_A$	$-2/\sqrt{3}\, v_{ca}$	p/6	$-2/\sqrt{3}\, i_A$	7p/6
+4	b	a	b	$-v_{ab}$	v_{ab}	0	i_B	$-i_B$	0	$2/\sqrt{3}\, v_{ab}$	5p/3	$2/\sqrt{3}\, i_B$	-p/6
-4	a	b	a	v_{ab}	$-v_{ab}$	0	$-i_B$	i_B	0	$-2/\sqrt{3}\, v_{ab}$	5p/3	$-2/\sqrt{3}\, i_B$	-p/6
+5	c	b	c	$-v_{bc}$	v_{bc}	0	0	i_B	$-i_B$	$2/\sqrt{3}\, v_{bc}$	5p/3	$2/\sqrt{3}\, i_B$	p/2
-5	b	c	b	v_{bc}	$-v_{bc}$	0	0	$-i_B$	i_B	$-2/\sqrt{3}\, v_{bc}$	5p/3	$-2/\sqrt{3}\, i_B$	p/2
+6	a	c	a	$-v_{ca}$	v_{ca}	0	$-i_B$	0	i_B	$2/\sqrt{3}\, v_{ca}$	5p/3	$2/\sqrt{3}\, i_B$	7p/6
-6	c	a	c	v_{ca}	$-v_{ca}$	0	i_B	0	$-i_B$	$-2/\sqrt{3}\, v_{ca}$	5p/3	$-2/\sqrt{3}\, i_B$	7p/6
+7	b	b	a	0	$-v_{ab}$	v_{ab}	i_C	$-i_C$	0	$2/\sqrt{3}\, v_{ab}$	3p/2	$2/\sqrt{3}\, i_C$	-p/6
-7	a	a	b	0	v_{ab}	$-v_{ab}$	$-i_C$	i_C	0	$-2/\sqrt{3}\, v_{ab}$	3p/2	$-2/\sqrt{3}\, i_C$	-p/6
+8	c	c	b	0	$-v_{bc}$	v_{bc}	0	i_C	$-i_C$	$2/\sqrt{3}\, v_{bc}$	3p/2	$2/\sqrt{3}\, i_C$	p/2
-8	b	b	c	0	v_{bc}	$-v_{bc}$	0	$-i_C$	i_C	$-2/\sqrt{3}\, v_{bc}$	3p/2	$-2/\sqrt{3}\, i_C$	p/2
+9	a	a	c	0	$-v_{ca}$	v_{ca}	$-i_C$	0	i_C	$2/\sqrt{3}\, v_{ca}$	3p/2	$2/\sqrt{3}\, i_C$	7p/6
-9	c	c	a	0	v_{ca}	$-v_{ca}$	i_C	0	$-i_C$	$-2/\sqrt{3}\, v_{ca}$	3p/2	$-2/\sqrt{3}\, i_C$	7p/6
0_a	a	a	a	0	0	0	0	0	0	0	--	0	--
0_b	b	b	b	0	0	0	0	0	0	0	--	0	--
0_c	c	c	c	0	0	0	0	0	0	0	--	0	--
---	a	b	c	v_{ab}	v_{bc}	v_{ca}	i_A	i_B	i_C	v_i	α_i	i_o	b_o
---	a	c	b	$-v_{ca}$	$-v_{bc}$	$-v_{ab}$	i_A	i_C	i_B	$-v_i$	$-\alpha_i+4p/3$	i_o	$-b_o$
---	b	a	c	$-v_{ab}$	$-v_{ca}$	$-v_{bc}$	i_B	i_A	i_C	$-v_i$	$-\alpha_i$	i_o	$-b_o+2p/3$
---	b	c	a	v_{bc}	v_{ca}	v_{ab}	i_C	i_A	i_B	v_i	$\alpha_i+4p/3$	i_o	$b_o+2p/3$
---	c	a	b	v_{ca}	v_{ab}	v_{bc}	i_B	i_C	i_A	v_i	$\alpha_i+2p/3$	i_o	$b_o+4p/3$
---	c	b	a	$-v_{bc}$	$-v_{ab}$	$-v_{ca}$	i_C	i_B	i_A	$-v_i$	$-\alpha_i+2p/3$	i_o	$-b_o+4p/3$

In order to make things easier for the reader and the writer, hereinafter any space vector will be simply referred as vector.

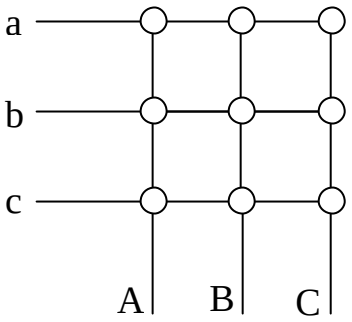

Fig.4.3 Matrix converter scheme for encoding configurations.

4.3 Space vector modulation applied to Matrix Converter control

The space vector modulation (SVM) is a control technique that has been widely used in adjustable speed drives and more generally in power converter control. In conventional DC-link voltage inverter applications the target of the SVM technique is to provide the desired or reference output voltage vector $\bar{v}_o$ using the voltage vectors generated by the different inverter configurations.

In the matrix converter case the SVM technique still point to provide the desired output voltage vector but due to the higher number of configurations available it can also control the phase angle of the input current vector $\bar{i}_i$.

Several control strategies based on SVM technique have been proposed in literature for the matrix converter.

In the control scheme proposed in [13] only synchronous and zero configurations are used. The scheme is simple to implement digitally and able to provide input power factor control and maximum voltage transfer ratio, but it requires a number of supply input phases at least of 6, in order to produce acceptable motor losses and torque pulsations.

In [14] a control scheme which make use of synchronous configurations only is proposed for a three-phase to three-phase matrix converter and experimentally proved. However, the scheme does not compensate for input disturbances and the polarity consistency rule is not respected leading to higher harmonic distortion of the output voltages and input currents.

All the control strategies presented in this chapter make use of the 18 active and the 3 zero configurations only. In Fig.4.4 and Fig.4.5 the output voltage and input current vectors corresponding to the 18 active and 3 zero configurations are shown and how the Gauss plane is divided in sectors is indicated.

It has been said that in matrix converter the aim of the SVM control algorithm is to generate the desired output line-to-line vector $\bar{v}_o$ and the input line current vector phase angle b_i which set the input power factor. An important point worth noting with regard to the input current vector is that only the phase angle b_i can be controlled. This is due to the fact that the matrix converter has no internal energy storage components. As a consequence, neglecting the switching losses, the instantaneous input power to the converter equals the instantaneous output power to the load. Using the space vector representation, this matrix converter inherent power balance can be expressed as

$$p_i = \frac{3}{2}\bar{e}_i \cdot \bar{i}_i = p_o \tag{4.14}$$

where the input line-to-neutral voltage vector $\bar{e}_i$ is defined, consistently to equation (4.1), by the following expression [11]

$$\bar{e}_i = \frac{1}{\sqrt{3}}\,\bar{v}_i\, e^{-j\frac{\pi}{6}} \tag{4.15}$$

Equation (4.14) establishes that for a given output power and input voltage vector, which is impressed by the AC mains supply, there are infinite possible solutions for the input current vector. On the contrary, if we define the phase angle of $\bar{i}_i$ by a suitable modulation of the converter, the power balance equation provides the complete determination of the input current vector.

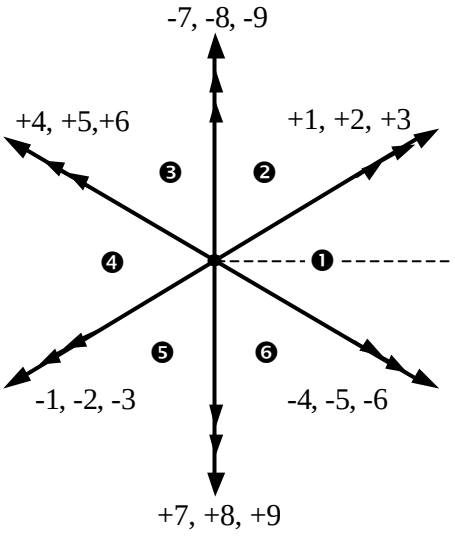

Fig.4.4 Output voltage space vectors for active and zero configurations

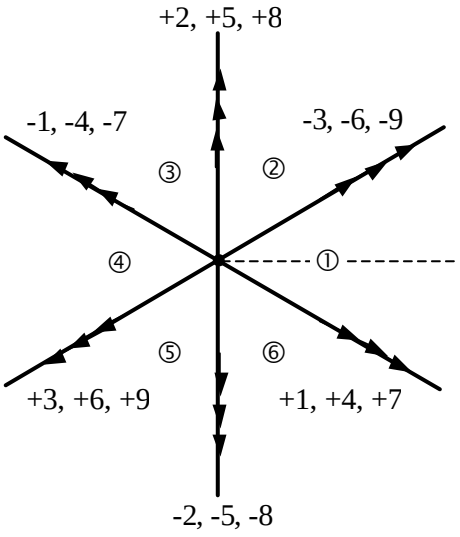

Fig.4.5 Input current space vectors for active and zero configurations

In principle, the SVM algorithm is based on the selection of four active configurations which are applied for suitable timewidths within each cycle period t_C. A zero configuration is then applied to complete t_C.

In order to explain the basic modulation algorithm, reference will be made to Fig.4.6 and Fig.4.7, where $\bar{v}_o$ and $\bar{i}_i$ are both lying in sector 1. This assumption does not affect the general validity of the analysis.

At any cycle period, the output voltage vector $\bar{v}_o$ and the input current displacement angle j_i are known as reference quantities. Since the input line-to-neutral voltage vector $\bar{e}_i$ is imposed by the source voltages and is also known by measurements, the control of j_i can be achieved controlling the phase angle b_i of the input current vector, as it can be easily understood by Fig.4.7.

In Fig.4.6 the reference voltage $\bar{v}_o$ is resolved into the components $\bar{v}_o'$ and $\bar{v}_o''$ along the two adjacent vector directions. The $\bar{v}_o'$ component can be synthesized using two voltage vectors having the same directions of $\bar{v}_o'$. Between the six possible matrix converter switches configurations (±1, ±2, ±3), the ones that allow the modulation of the input current direction, also, have to be chosen. It is verified that this constraint allows the elimination of two

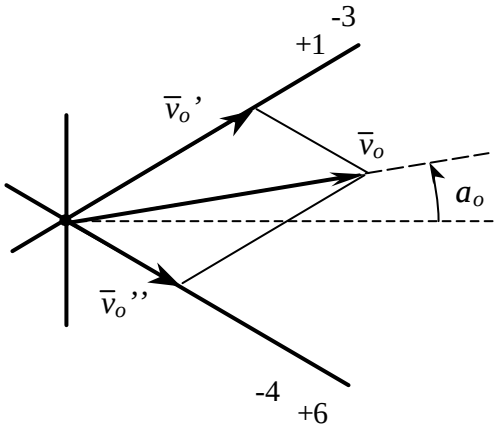

Fig.4.6 Space vector modulation of the reference output voltage vector.

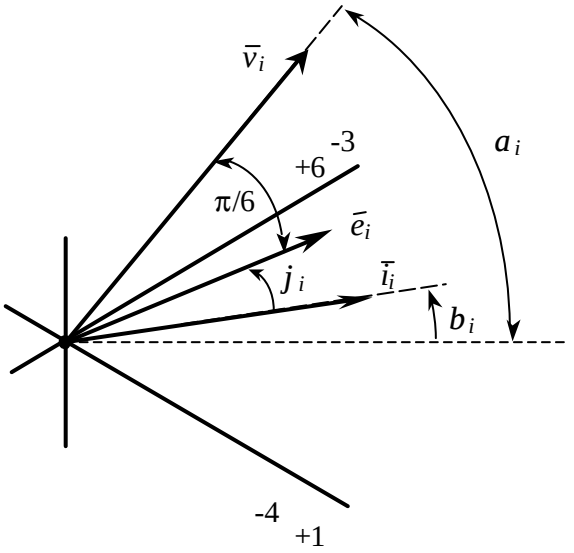

Fig.4.7 Space vector modulation of the reference input current phase angle.

configurations, +2 and –2 in this case. Among the remaining four, the two switches configurations giving higher voltage values are chosen to be applied, +1 and –3 in the case. Likewise, the matrix converter switches configurations required to synthesized the $\bar{v}_o''$ component can be also determined, being in the case –4 and +6.

Using the same procedure, it is possible to determine the four switches configurations correspondent to any possible combination of output voltage and input current sectors, which are quoted in Table II. The last row symbols are introduced in order to identify each switches configuration for a given couple of sector values.

Table II

Matrix configurations for each combination of output voltage and input current sector.

v_o / i_i	❶	❷	❸	❹	❺	❻
①	-3 +1 +6 -4	+9 -7 -3 +1	-6 +4 +9 -7	+3 -1 -6 +4	-9 +7 +3 -1	+6 -4 -9 +7
②	+2 -3 -5 +6	-8 +9 +2 -3	+5 -6 -8 +9	-2 +3 +5 -6	+8 -5 -2 +3	-5 +6 +8 -9
③	-1 +2 +4 -5	+7 -8 -1 +2	-4 +5 +7 -8	+1 -2 -4 +5	-7 +8 +1 -2	+4 -5 -7 +8
④	+3 -1 -6 +4	-9 +7 +3 -1	+6 -4 -9 +7	-3 +1 +6 -4	+9 -7 -3 +1	-6 +4 +9 -7
⑤	-2 +3 +5 -6	+8 -5 -2 +3	-5 +6 +8 -9	+2 -3 -5 +6	-8 +5 +2 -3	+5 -6 -8 +9
⑥	+1 -2 -4 +5	-7 +8 +1 -2	+4 -5 -7 +8	-1 +2 +4 -5	+7 -8 -1 +2	-4 +5 +7 -8
	I II III IV	I II III IV	I II III IV	I II III IV	I II III IV	I II III IV

Now, it is possible to write in a general form the basic equations of the SVM algorithm which satisfy, at the same time, the requirements for the reference output voltage vector and the input displacement angle. These equations can be written as

$$\bar{v}_o' = \bar{v}_o^I d^I + \bar{v}_o^{II} d^{II} = \frac{2}{\sqrt{3}} v_o \cos\left(\tilde{\alpha}_o - \tfrac{\pi}{3}\right) e^{j[(K_v-1)\pi/3 + \pi/6]} \tag{4.16}$$

$$\bar{v}_o'' = \bar{v}_o^{III} d^{III} + \bar{v}_o^{IV} d^{IV} = \frac{2}{\sqrt{3}} v_o \cos\left(\tilde{\alpha}_o + \tfrac{\pi}{3}\right) e^{j[(K_v-1)\pi/3 - \pi/6]} \tag{4.17}$$

$$(\bar{i}_i^I d^I + \bar{i}_i^{II} d^{II}) \cdot j i_i e^{j\tilde{\beta}_i} = 0 \tag{4.18}$$

$$(\bar{i}_i^{III} d^{III} + \bar{i}_i^{IV} d^{IV}) \cdot j i_i e^{j\tilde{\beta}_i} = 0 \tag{4.19}$$

where d^I, d^{II}, d^{III}, d^{IV} are the on-time ratio (i.e. $d^I = t^I / t_C$) of the four configurations and K_v = 1, 2, …., 6 represents the output voltage sector. v^I, v^{II}, v^{III}, v^{IV} are the output voltage vectors associated, respectively, with the switches configurations I, II, III and IV given in Table II. The same formalism is used for the input current vectors.

In equations (4.16) - (4.19) $\tilde{\alpha}_o$ and $\tilde{\beta}_i$ are the output voltage and input current phase angle referred to the bisecting line of the corresponding sector. In equations (4.18) and (4.19) the scalar product imposes the input current vector along the desired direction.

Solving equations (4.16)-(4.19) with respect to the on-time ratios, after some formulae manipulations, leads to the following relationships:

$$d^I = \frac{2}{\sqrt{3}} \frac{v_o}{v_i} \frac{\cos\left(\tilde{\alpha}_o - \tfrac{\pi}{3}\right) \cos\left(\tilde{\beta}_i - \tfrac{\pi}{3}\right)}{\cos\varphi_i} \tag{4.20}$$

$$d^{II} = \frac{2}{\sqrt{3}} \frac{v_o}{v_i} \frac{\cos\left(\tilde{\alpha}_o - \tfrac{\pi}{3}\right) \cos\left(\tilde{\beta}_i + \tfrac{\pi}{3}\right)}{\cos\varphi_i} \tag{4.21}$$

$$d^{III} = \frac{2}{\sqrt{3}} \frac{v_o}{v_i} \frac{\cos\left(\tilde{\alpha}_o + \tfrac{\pi}{3}\right) \cos\left(\tilde{\beta}_i - \tfrac{\pi}{3}\right)}{\cos\varphi_i} \tag{4.22}$$

$$d^{IV} = \frac{2}{\sqrt{3}} \frac{v_o}{v_i} \frac{\cos\left(\tilde{\alpha}_o + \tfrac{\pi}{3}\right) \cos\left(\tilde{\beta}_i + \tfrac{\pi}{3}\right)}{\cos\varphi_i} \tag{4.23}$$

Equations (4.20)-(4.23) have a general validity. For any combination of the output voltage sector K_v and the input current sector K_i Table II provides the four switches configurations to be used within the cycle period t_C and equations (4.20)-(4.23) give the correspondent on-time ratios.

In equations (4.20)-(4.23) the following angle limits apply:

$$-\frac{\pi}{6} < \tilde{\alpha}_o < +\frac{\pi}{6}, \qquad -\frac{\pi}{6} < \tilde{\beta}_i < +\frac{\pi}{6} \tag{4.24}$$

For the feasibility of the control algorithm, the sum of the four on-time ratios must be lower than or equal to unity:

$$d^{I} + d^{II} + d^{III} + d^{IV} \leq 1 \tag{4.25}$$

A zero configuration is applied to complete the sampling period. If equations (4.20)-(4.23) are substituted in (4.25), after some formulae manipulations, the following equation can be obtained:

$$v_o \leq v_i \frac{\sqrt{3}}{2} \frac{\left|\cos\varphi_i\right|}{\cos\tilde{\alpha}_o \cos\tilde{\beta}_i} \tag{4.26}$$

This is a significant equation. What is on the right hand side of the equation is, at any instant, the theoretical maximum limit for the output voltage vector magnitude, which depends on the instantaneous input voltage vector magnitude, the output voltage and input current vectors phase angle and the reference displacement angle of the input current vector.

The equation (4.26) is very useful in order to define the performance limits of the matrix converter when not-ideal input voltage conditions exist on the AC mains supply or when a dynamic control of the output voltage vector is required, as for high-performance AC drives.

It is worth noting that, in the particular case of balanced and sinusoidal supply voltage conditions, if balanced output voltages have to be generated, the usual maximum modulation depth occurs when the right hand side term of (4.26) is a minimum, which occurs when $\cos\tilde{\alpha}_o$ and $\cos\tilde{\beta}_i$ are equal to 1. In this case equation (4.26) leads to the following relation

$$V_o \leq V_i \frac{\sqrt{3}}{2} \left|\cos\varphi_i\right| \tag{4.27}$$

where V_o and V_i represent the constant values of the output and input voltage vector magnitude. When reference input power factor is set at unity, equation (4.27) gives the well known theoretical maximum voltage transfer ratio of matrix converters [7] under the constraint of sinusoidal input and output waveforms.

Equations (4.20)-(4.23) show that the implementation of the SVM algorithm requires, at any cycle period, the knowledge of the input line-to-line voltage vector $\bar{v}_i$. Therefore, two line-to-line input voltages have to be measured. For balanced and sinusoidal supply voltages this requirements is not necessary since the synchronization with the input voltages can be achieved by detecting the zero crossing of an input voltage.

4.4 Performance of a Matrix Converter under non ideal supply voltage conditions

In general, the matrix converter control algorithms are derived under the assumption that supply voltages are sinusoidal and balanced, but in practice the AC mains supply is usually unbalanced to a certain extent and distorted, due to the presence of non-linear loads connected to it. Due to the lack of an intermediate DC link and relevant energy storage components, the matrix converter is sensitive to these disturbances in the input voltages, as these will transmit directly to the output side of the converter.

As a consequence, a control algorithm, in order to be effective has to be able to provide a system of balanced and sinusoidal output voltages even under not ideal supply voltage conditions.

In [15]-[18] it has been demonstrated how it is possible to generate balanced and sinusoidal output voltages even when the input voltages are unbalanced. In [15] a detailed harmonic analysis of the matrix converter input current under unbalanced input voltages is carried out on the basis of a rigorous analytical approach. In [16] this analysis has been further developed in order to take also into account the output unbalance. Still using an analytical approach, in [17]-[18] two modulation strategies which differently perform in terms of harmonic content of the matrix converter input current have been investigated under unbalanced input voltage conditions.

In [19] the analysis of the input current harmonics has been extended to the case of unbalanced and nonsinusoidal input voltages by using a general approach based on the linearization of the matrix converter input/output equations. The advantage of this linearized analysis is to allow the investigation of the matrix converter performance under any condition determined by disturbances in the input supply voltages.

Hereinafter three modulation strategies will be presented and analyzed using the linearized approach. These strategies have similar performance with respect to the output voltages as they have the same output voltage reference vector, but they differently modulate the matrix converter input currents, since they define a different instantaneous displacement angle between the vectrors $\bar{i}_i$ and $\bar{e}_i$. As a consequence they give rise to different low order harmonic spectra of the input currents when disturbances exist in the input supply voltages.

4.4.1 Analysis of the input current low order harmonics

As direct type power converter the matrix converter does not have internal storage energy. Making the assumption of ideal switches the input power flow equals the output power flow at any instant, then it holds

$$\frac{3}{2}\bar{e}_i \cdot \bar{i}_i = \frac{3}{2}\bar{e}_o \cdot \bar{i}_o \tag{4.28}$$

where $\bar{e}_i$, $\bar{i}_i$,$\bar{e}_o$,$\bar{i}_o$ are the instantaneous space vector representation of the input and output line-to-neutral voltages and currents accordingly to equations (4.10)-(4.13) and (4.15) and ($\times$) denotes the scalar product.

This power balance is the basis of the analysis presented in this section. Equation (4.28) also clearly shows that if the output power is kept constant, generating a sinusoidal and balanced output voltage system, any distortion and/or unbalance in the input voltage vector $\bar{e}_i$ necessarily translates in a distortion and/or unbalance of the input current vector.

The following analytical developments are carried out under the assumption of neglecting the effects of the switching harmonics and considering for the output voltages and input currents their average values over a cycle period. This assumption is deemed acceptable since the analysis is focused on harmonic current components at frequencies much lower than the usual switching frequency of matrix converters.

Bearing in mind that modulating the input current vector means to define its reference phase angle, it is assumed that the input current vector is modulated along the direction of an arbitrary space vector $\bar{\psi}$, named modulation vector. Then, the following equation can be written

$$\bar{\psi} \cdot j\bar{i}_i = 0 \tag{4.29}$$

Solving (4.28) and (4.29) with respect to $\bar{i}_i$ leads to

$$\bar{i}_i = \frac{4}{3}\frac{p_o}{\bar{e}_i\,\bar{\psi}^* + \bar{e}_i^*\,\bar{\psi}}\bar{\psi} \tag{4.30}$$

where $\bar{e}_i^*$ is the complex conjugate of the input line-to-neutral voltage vector and p_o is the instantaneous output power, given by the expression

$$p_o = \frac{3}{2}\bar{e}_o \cdot \bar{i}_o \tag{4.31}$$

Operating the matrix converter in order to generate balanced output voltages on a balanced load, the output power assumes a constant value, indicated in the following by P_o. Equation (4.30) gives a general relationship for the input current vector expressed as a function of the output power, the input voltage vector and the modulation vector. With regard to equation (4.30) it is important to note that, consistently to what aforementioned, the input current vector is not affected by the amplitude of $\bar{\psi}$, but only by its phase angle. The relation (4.30) can be further developed once the modulation law for the input current is specified.

As an example, if the input current vector is modulated in order to be, at any instant, in phase with the input voltage vector $\bar{e}_i$, it can be assumed

$$\bar{\psi} = \bar{e}_i \tag{4.32}$$

This choice determines unity input power factor. By substitution of (4.32) in (4.30) it is obtained

$$\bar{i}_i = \frac{2\,P_o}{3\bar{e}_i^*} \tag{4.33}$$

On the basis of equation (4.33), the input current can be easily determined by numerical analysis once the input voltage vector is known.

4.4.2 Linearized analysis

The limit of the analytical approach used in [15]-[18] for analyzing the input current quality under non-ideal supply voltages conditions is the practicability to get a solution only if just one extra component is considered in addition to the positive sequence fundamental one [19].

The advantage of the linearized analysis is the possibility to deal with more complicated non-ideal supply voltages conditions at the expense of a slight approximation, as it has been demonstrated in [19]. The linearized analysis holds for practical values of the supply voltage disturbances and provides an approximate solution of the input current harmonic content. For the sake of clarity, the term “disturbance” will be used hereinafter either to indicate the negative sequence fundamental component or a harmonic component.

The linearized approach is based on the linearization of the matrix converter input-output equations. The analysis assumes that the input voltage vector is given by two terms, the first representing a system of balanced and sinusoidal input voltages and the second representing a small input voltage vector disturbance. Accordingly to these assumptions, the input line-to-neutral voltage vector can be written as

$$\bar{e}_i = \overline{E}_{i_1} e^{j\omega_i t} + D\bar{e}_i \tag{4.34}$$

In the same way, the input current vector is given by

$$\bar{i}_i = \frac{2P_o}{3\overline{E}_{i_1}^*} e^{\,j\omega_i t} + D\bar{i}_i \tag{4.35}$$

In equation (4.35) the first term represents balanced and sinusoidal currents with unity input power factor. The second represents the input current disturbance.

In similar way, the modulation vector $\overline{\psi}$ along which the input current vector is modulated can be expressed as

$$\overline{\psi} = \overline{E}_{i_1} e^{\,j\omega_i t} + D\overline{\psi} \tag{4.36}$$

In Fig.4.8 a representation of the above defined space vectors and its components is given. If the equations (4.34) and (4.36) are substituted in the general expression (4.30), after some manipulation and neglecting the second-order effects the following expression is obtained

$$\bar{i}_i = \frac{2P_o}{3\overline{E}_{i_1}^*} e^{j\omega_i t} + \frac{P_o}{3\left|\overline{E}_{i_1}\right|^2}\left(D\overline{\psi} - D\bar{e}_i\right) - \frac{P_o}{3\overline{E}_{i_1}^{*\,2}} e^{j2\omega_i t}\left(D\overline{\psi}^* + D\bar{e}_i^*\right) \tag{4.37}$$

Equation (4.37) shows that the input current vector consists of three terms. The first term represents the input current vector which would be generated if the input voltage system was balanced and sinusoidal, likewise to equation (4.35). The second and third terms represent the input current disturbance due to the input voltage vector disturbance. When the modulation strategy is established, these terms can be further developed.

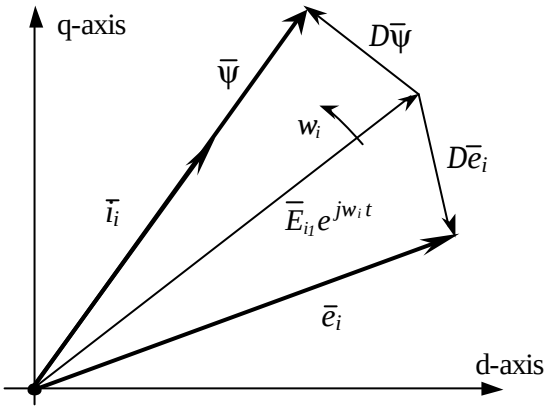

Fig.4.8 Representation of the input space vectors.

Looking at equation (4.37) two possible input current modulation strategies can be easily identified. The first is defined by $D\overline{\psi} = D\bar{e}_i$ and allows to cancel the first disturbance term. The second strategy is defined by $D\overline{\psi} = -D\bar{e}_i$ and allows to cancel the second disturbance term in (4.37). But many other strategies could be chosen to define the instantaneous displacement angle between $\bar{e}_i$ and $\bar{i}_i$. A third strategy that might be used is defined by $D\overline{\psi} = 0$.

In the following, the effects of these three strategies on the input current spectrum will be analyzed. With this object in view, it is opportune to express the input voltage and current disturbances by their complex Fourier series expansion as follows:

$$D\bar{e}_i = \sum_{-\infty}^{+\infty}{}_{k\neq 1} D\overline{E}_{i_k} e^{j k \omega_i t} \tag{4.38}$$

$$D\bar{i}_i = \sum_{-\infty}^{+\infty}{}_{k} \bar{I}_{i_k} e^{j k \omega_i t} \tag{4.39}$$

Equations (4.38) and (4.39) represents any type of input voltage disturbance.

Furthermore, having the aim to discuss the performance of the three strategies in terms of input current quality, the following evaluation parameters are defined

$$D\,i_{i_{RMS}} = \sqrt{\frac{3}{2}} \sqrt{\sum_{-N}^{+N}{}_k \left| D\,\bar{I}_{i_k} \right|^2} \tag{4.40}$$

$$I_{3_{RMS}} = \sqrt{\frac{3}{2}} \sqrt{\sum_{-N}^{+N}{}_k \bar{I}_{i_k}^2} \tag{4.41}$$

$D\,i_{i_{RMS}}$ is the root mean square (RMS) value of the input current disturbance $D\,\bar{i}_i$ and $I_{3_{RMS}}$ is the three phase RMS value of the matrix converter input currents, both calculated on the basis of a finite number N of positive and negative harmonic components.

4.4.3 Modulation strategy A

Modulation strategy A can be utilized in order to keep, at any instant, the input current vector $\bar{i}_i$ in phase with the input line-to-neutral voltage vector $\bar{e}_i$. This means that the input power factor is instantaneously kept at unity. Such operating condition is represented by

$$D\,\overline{\psi} = D\,\bar{e}_i \tag{4.42}$$

From equations (4.34) and (4.36) this means that

$$\overline{\psi} = \bar{e}_i \tag{4.43}$$

accordingly to what said above. If taking into account equation (4.38), equation (4.42) is substituted in equation (4.37), the following expression is obtained for the input current vector.

$$\bar{i}_i = \frac{2P_o}{3\overline{E}^*_{i_1}} e^{\,j\omega_i t} - \frac{2P_o}{3\overline{E}^{*2}_{i_1}} \sum_{-\infty}^{+\infty}{}_{k\neq 1}\; D\,\overline{E}^*_{ik}\; e^{\,j(2-k)\omega_i t} \tag{4.44}$$

Equation (4.44) clearly shows the direct correlation between the input current and the input voltage harmonic content. It can be noted that the *k*th harmonic component in the input voltage disturbance produces a harmonic component in the input current of order 2 - *k*. In the case of unbalanced sinusoidal supply voltages (*k* = -1), for instance, the input current disturbance is represented by a third harmonic component and the ratio of its magnitude to the fundamental is equal to the input voltage disturbance one.

4.4.4 Modulation strategy B

Modulation strategy B has been defined with the purpose of reducing, compared to strategy A, the harmonic content of the input currents under unbalanced input supply voltage conditions [18]. The operating condition of this starategy is defined by

$$D\,\overline{\psi} = -D\,\overline{e}_i \tag{4.45}$$

From equations (4.34) and (4.36) this means that

$$\overline{\psi} = \overline{e}_i - 2D\,\overline{e}_i \tag{4.46}$$

By equation (4.46) it is evident that strategy B does not keep the input power factor at unity istantaneously but it carries out a dynamic modulation of the input current diplacement angle. Fig.4.9 better explains the concept of dynamic modulation.

Substituting the modulation law expressed by (4.45) in equation (4.37) and taking into account equation (4.38), the input current vector reduces to the following expression

$$\overline{i}_i = \frac{2P_o}{3\overline{E}^{*}_{i_1}} e^{\,j\omega_i t} - \frac{2P_o}{3\left|\overline{E}_{i_1}\right|^2} \sum_{-\infty}^{+\infty}{}_{k\neq 1}\; D\overline{E}_{i_k}\; e^{\,j\,k\,\omega_i t} \tag{4.47}$$

In this case also, it is evident the direct correlation between the input current and the input voltage harmonic content. It can be noted that the *k*th harmonic component in the input voltage disturbance produces a harmonic component in the input current of the same harmonic order. It is interesting to note that under unbalanced sinusoidal supply voltages (k = -1), the input current disturbance is represented by only the negative sequence fundamental component. This means that compared to strategy A, under unbalanced sinusoidal supply voltages, strategy B provides input currents with sinusoidal waveforms at the expense of a certain degree of unbalance.

But if the negative sequence fundamental component of the input currents is considered as a disturbance, then the RMS value of the input-current disturbance assume the same values of strategy A [19].

4.4.5 Modulation strategy C

Modulation strategy C has been proposed in [19] as the optimal modulation strategy that under any supply voltages disturbances minimizes the generated input currents disturbances. The operating condition of this starategy is simply defined by

$$D\;\overline{\psi} = 0 \tag{4.48}$$

From equations (4.34) and (4.36) it follows that

$$\overline{\psi} = \overline{E}_{i_1} e^{j\omega_i t} \tag{4.49}$$

Accordingly to equation (4.49), using strategy C the input current vector is modulated in phase with the vector corresponding to the input voltage positive sequence fundamental component. As a consequence, in a similar way to strategy B, the input power factor is not controlled to be istantaneously at unity.

Substituting the modulation law expressed by (4.48) in equation (4.37) by way of equation (4.38), the input current vector reduces to the following expression

$$\overline{i}_i = \frac{2P_o}{3\overline{E}^*_{i_1}} e^{j\omega_i t} - \frac{P_o}{3\left|\overline{E}_{i_1}\right|^2} \sum_{-\infty}^{+\infty}{}_{k\neq 1} D\overline{E}_{i_k} e^{jk\omega_i t} - \frac{P_o}{3\left|\overline{E}_{i_1}\right|^2} \sum_{-\infty}^{+\infty}{}_{k\neq 1} D\overline{E}^*_{i_k} e^{j(2-k)\omega_i t} \tag{4.50}$$

Equation (4.50) states that a harmonic component of order k in the input voltage vector disturbance produces two input current harmonic components of order k and $2 - k$, which have the same amplitude. But what is important to note is that the amplitude of these input current harmonic components is one half of the harmonic components given by strategy A in (4.44) and strategy B in (4.47). The effect is a reduction with respect to strategies A and B of the rms value of the input current disturbances as well as of the input current distortion factor [19].

<table>
<tr><td colspan="3">Unbalanced and Sinusoidal Input Voltages
$\overline{e}_i = \overline{E}_{i_1} e^{j\omega_i t} + \overline{E}_{i_{-1}} e^{-j\omega_i t} = \overline{e}_{i_1} + \overline{e}_{i_{-1}}$</td></tr>
<tr><td>Strategy A</td><td>Strategy B</td><td>Strategy C</td></tr>
<tr><td>$\overline{\psi} = \overline{e}_{i_1} + \overline{e}_{i_{-1}}$</td><td>$\overline{\psi} = \overline{e}_{i_1} - \overline{e}_{i_{-1}}$</td><td>$\overline{\psi} = \overline{e}_{i_1}$</td></tr>
<tr><td>The reference input displacement angle φ_i is constant and = 0</td><td>The reference input displacement angle φ_i is variable</td><td>The reference input displacement angle φ_i is constant and $\neq 0$</td></tr>
<tr><td> 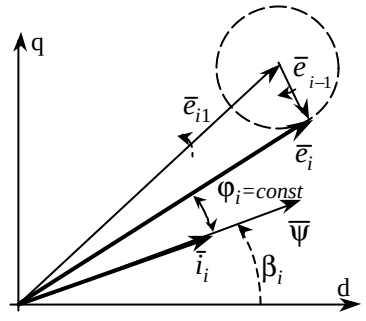
</td><td> 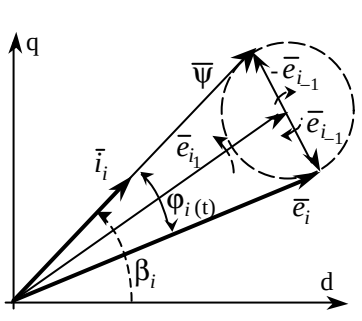
</td><td> 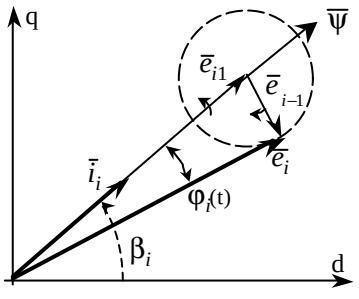
</td></tr>
</table>

Fig.4.9 Example of how the three strategies operate under unbalanced and sinusoidal supply voltages.

Some remarks can be made with reference to Fig.4.9.

Looking at the modulation vector $\overline{\psi}$ it can be noted that under sinusoidal and balanced input voltages condition vector its expression is the same for the three strategies, which modulate the input current in order to be istantaneously in phase with the input line-to-neutral voltage vector $\overline{e}_i$, that means $\varphi_i = 0$. But when a disturbance exists on the input voltages this is no longer valid for strategies B and C.

For strategy B the modulation vector has a circular motion around the vector $\overline{e}_i$ which brings the input displacement angle j_i to oscillate within the range $\pm arctg\, \overline{e}_{i_{-1}} / \overline{e}_{i_1}$. In this case it is the mean value of the input displacement angle j_i on the fundamental period to be equal to zero.

For strategy C is the input voltage vector $\overline{e}_i$ that has a circular motion around the modulation vector but the effect on the input displacement angle j_i is the same.Then, for strategy C too, the input displacement angle j_i is equal to zero on the fundamental period average.

From this perspective, strategies B and C with respect to strategy A might be viewed as dynamic modulation strategies.

4.5 Validation of the three modulation strategies

The core of the research activity carried out during the dottorato course has been concentrated on the validation of the theretical results above presented. In [18] and [19] the performance of the three strategies in terms of input current quality have been verified by means of numerical simulations carried out on the basis of a simplified model of a matrix converter system.

The model assumed an AC mains supply of infinite power, that means zero series impedance, and did not take into account any kind of input filter. Although these assumptions were not expected to affect the validity of the linearized analysis results, they established some operating problems.

First, in a real matrix converter system it would have been really complicated, if still possible, to measure the matrix converter input currents, because of accessability problems to the point of measurement.

Second, a real matrix converter does need an input filter and how this input filter interacts with the matrix converter and with the AC main supply is hardly straightforward to predict.

Third, the lack of an AC mains impedance as well as of an input filter in the simplified model did not allow to evaluate the effect, if any significant, of the input current disturbances injected by the matrix converter on the input voltages.

On the basis of these consideratons a new mathematical model of a matrix converter system has been developed. Moreover, it has been decided to evaluate the performance of the three modulation strategies also on the basis of the input line currents instead of the converter

input currents. This choice was also dictated by the fact that in actual systems the standards set limits for the power factor and the harmonic distortion at the point of common coupling.

Consistently to this choice and the above considerations, in order to compare the performance of the three modulation strategies in terms of input power quality the following two evaluation parameters have been also considered:

$$HD_N = \frac{\sqrt{\sum_{k=2}^{N} I_{k\,max}}}{I_{1\,max}} \tag{4.51}$$

$$I_{3_{RMS}} = \sqrt{\frac{1}{T}\int_0^T (\, i_a^2 + i_b^2 + i_c^2 \,)\, dt} \tag{4.52}$$

The first parameter HD_N is the harmonic distortion factor of the input line currents calculated with respect to the first N harmonic components, with N =11 and N =15, in order to give more evidence to the region of the harmonic spectrum in which the strategies are expected to be effective.

The second parameter I_{3RMS} is the three phase RMS value of the three phase input line currents system defined as in [12]. This expression is equivalent to equation (4.41) but it allows to calculate the three phase RMS value by simply measuring the RMS value of the input currents.

4.5.1 Mathematical model of a Matrix Converter control system

In Fig.4.10 it is shown the schematic circuit of the matrix converter system that has been modelized.

As far as the matrix converter is concerned it is assumed that the commutations are instantaneous and ideal, that means no losses: the bi-directional switches are ideal.

The AC mains supply has finite power. It is a matter of fact that neglecting supply impedance might give misleading results since it affect the overall impedance seen by the input side of the converter.

For the input filter a second order L-C configuration with damping parallel resistor has been chosen as more general solution. This choice has been made on the basis of a survey of the most commonly used input filter configurations in matrix converter systems and drives [1]-[10] and in order to investigate how the input filter parameters affect the performance of the control system and what is, if any, the optimal solution.

With regard to the output load, a three phase ohmic-inductive passive load has been considered.

The numerical or mathematical model has been implemented using the MS-FORTRAN 77 language. At each cycle period the switching configurations of the matrix converter to be applied, four active and one zero, are selected according to the SVM control algorithm outlined in section 4.3.

At the beginning of each cycle period the input and the output voltage vectors are known. Once the input current modulation strategy is chosen, it is possible to select the five switching configurations and calculate the corresponding on-time ratios. During the time width of each switching configuration, the input voltages, and then the output voltages, are assumed to be constant. Under these assumption, it is possible to solve analitycally the voltage equations of the load. In this way the switching effects have been taken into account. In order to obtain more realistic results, phenomena like the influence of the discretization and the sampling delay of the two input line-to-line voltages measurement has been also considered.

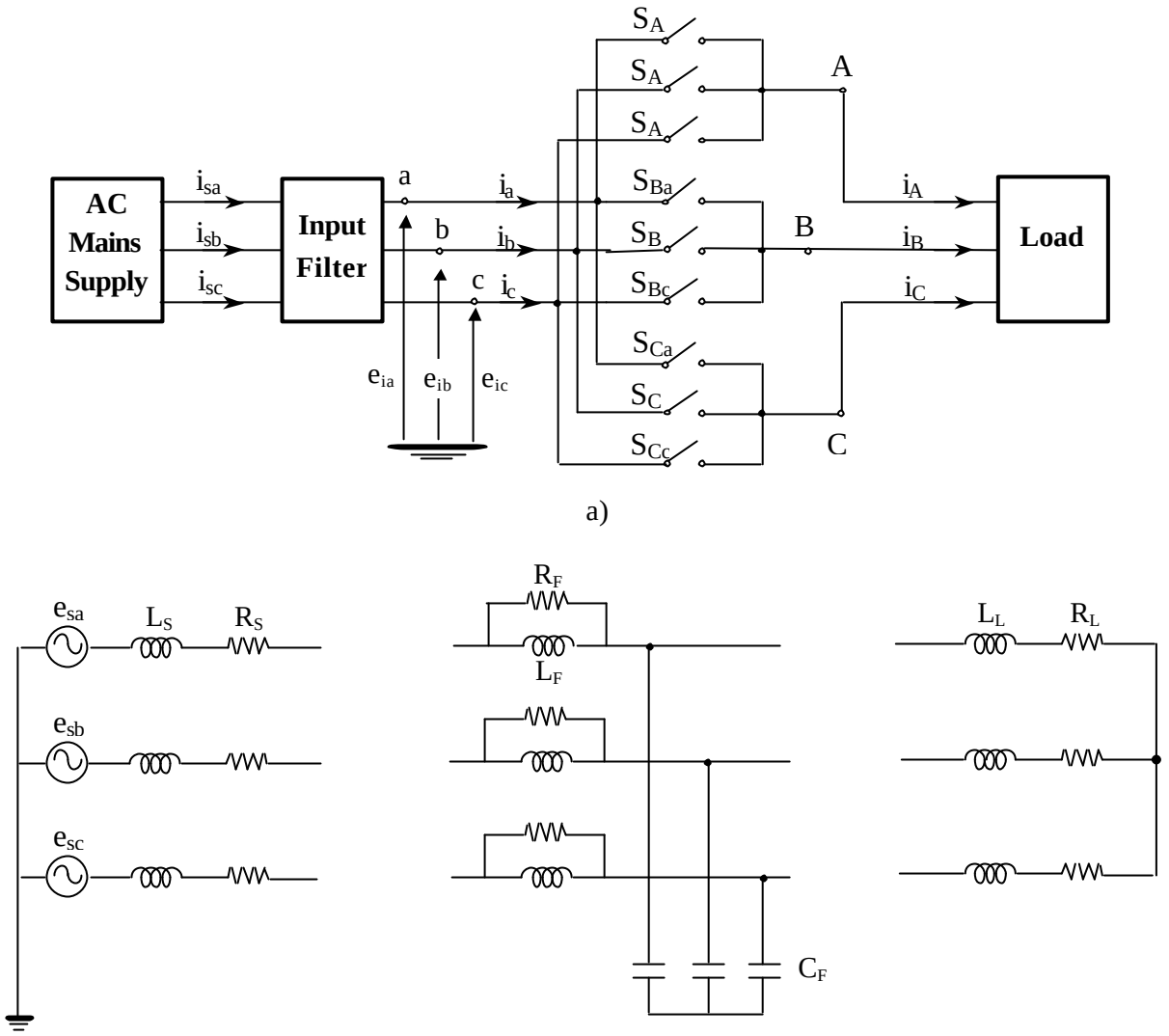

Fig.4.10 Schematic circuits of the modelized matrix converter system. a) Main block diagram. b) Three phase AC mains supply. c) LC input filter with damping parallel resistor. d) Three phase symmetrical R-L passive load.

An important point worth noting is related to how the selected configurations are applied within a cycle period and which is the sequential order of application. It is a matter of fact that the configurations switching sequence affects the harmonic spectrum of the output voltages and input currents as well as the converter switching losses [20]-[22]. In the numerical model it is assumed that the so called “double sided” configurations switching sequence [22] is used.

The cycle period of the control algorithm has been set to 250 μs. With regard to the output voltage a simple constant V/f control has been implemented.

The following Figs.4.11 - 4.18 have just the purpose to show the general performance of a matrix converter and to verify that the expectations are met. Some comments are also given. The AC mains supply is balanced and sinusoidal. The output to input voltage ratio is equal to $\cong 0.49$. The output frequency is 25 Hz. Strategy C is used. In Table III the system parameters value used for the simulations are quoted. It has to be noted that the input filter capacitance has been oversized.

Table III.
System parameters value used by simulations.

L_S [mH]	R_S [Ω]	R_F [Ω]	L_F [mH]	C_F [μF]	L_L [mH]	R_L [Ω]
0.277	0.14	∝	1.2	14	27	17

For Figs.4.10, 4.12, 4.14, 4.16 the matrix converter input power factor is controlled to be at unity since the reference input current vector phase displacement with respect to the input line-to-neutral voltage vector $\bar{e}_i$ is set to zero, $\varphi_i = 0$.

In the case of Figs.4.11, 4.13, 4.15, 4.17 the reference input current vector phase displacement is lagging the vector $\bar{e}_i$ by 15° degrees. This is evident looking at Figs.4.10 and 4.11.

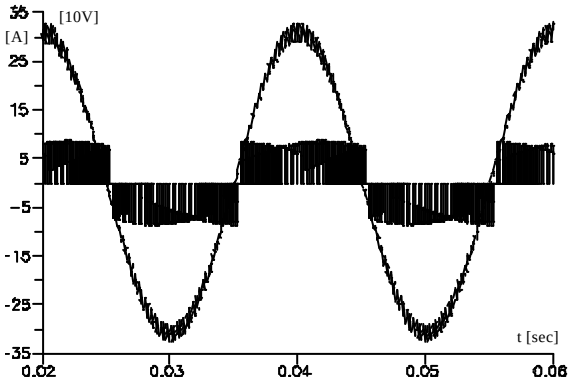

Fig.4.11 Input line-to-neutral voltage and relevant input current for φ_i=0.

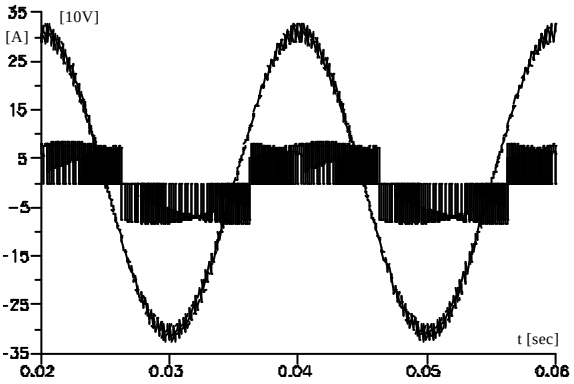

Fig.4.12 Input line-to-neutral voltage and relevant input current for φ_i=-15°.

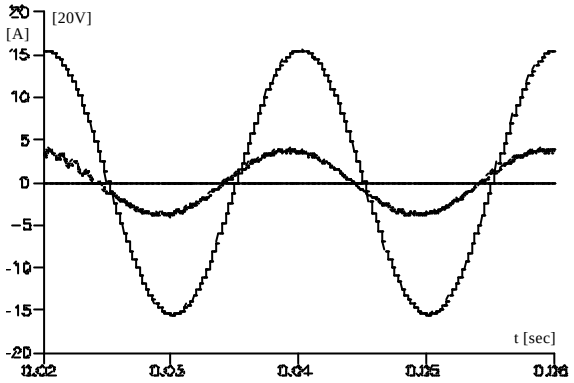

Fig.4.13 Supply line-to-neutral voltage and relevant input line current for φ_i=0.

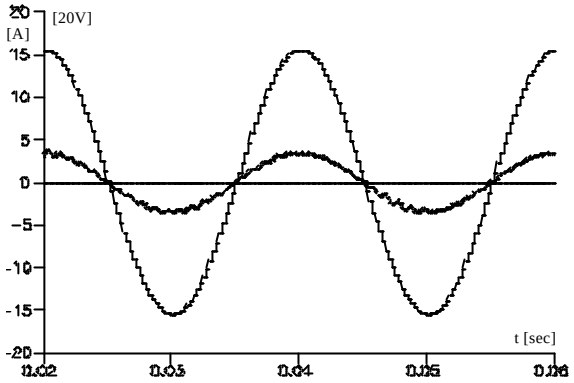

Fig.4.14 Supply line-to-neutral voltage and relevant input line current for φ_i=-15°.

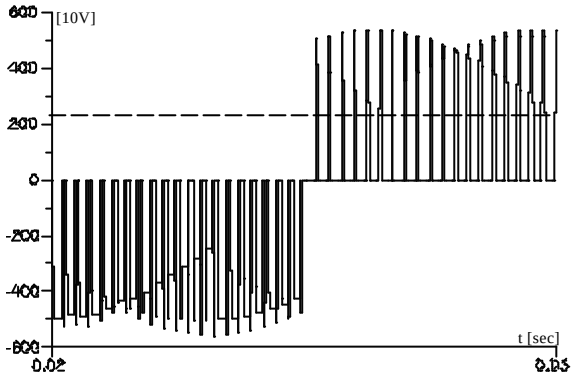

Fig.4.15 Output line-to-line voltage for φ_i=0.

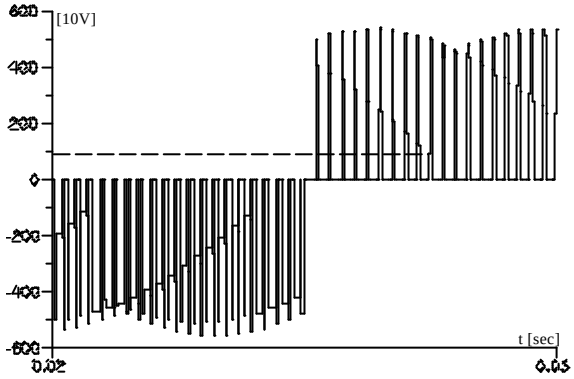

Fig.4.16 Output line-to-line voltage for φ_i=-15°.

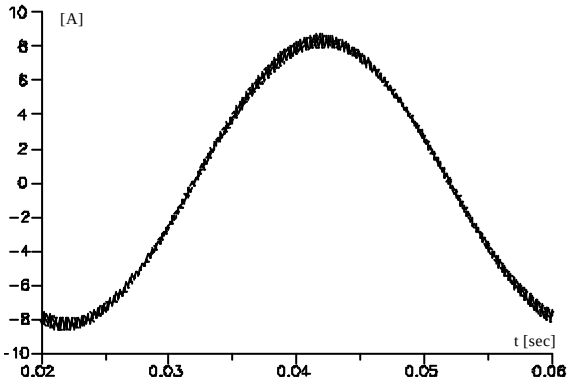

Fig.4.17 Output line current for φ_i=0.

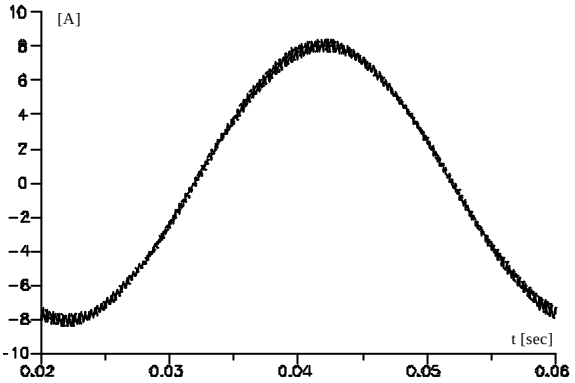

Fig.4.18 Output line current for φ_i=-15°.

For Figs.4.11, 4.13, 4.15, 4.17 the matrix converter input power factor is controlled to be at unity since the reference input current vector phase displacement with respect to the input line-to-neutral voltage vector $\bar{e}_i$ is set to zero, $\varphi_i = 0$.

In the case of Figs.4.12, 4.14, 4.16, 4.17 the reference input current vector phase displacement is lagging the vector $\bar{e}_i$ by 15° degrees. This is evident looking at Figs.4.11 and 4.12. It has to be noted that the control algorithm can modulate the phase angle of the matrix converter input current vector $\bar{i}_i$ only. As a consequence, if the matrix converter is controlled in

order to have unity input power factor, the input line currents, i.e. isa, isb and isc, will be always leading to some extent the correspondent supply line-to-neutral voltage, due to the current drawn by the input filter capacitors. Controlling the matrix converter input current in order to lag the voltage, as shown in Fig.4.12, it is possible to compensate the effect of the input filter capacitors current on the AC mains power factor, as shown in Fig.4.14.

But as said before, accordingly to equation (4.27), by choosing a reference phase displacement $\varphi_i \neq 0$ the maximum output to input voltage ratio available is reduced. Therefore, such compensation of the input filter capacitor current becomes effective only if there is a sufficient margin between the theoretical output voltage limit of the matrix converter and the maximum voltage level required by the load. Otherwise, the overmodulation operating region is entered with consequent distortion of the output and input waveforms.

The general approach to this problem is not to compensate the input filter capacitor current, because at the rated power its effect becomes negligible [6]-[11]. However, this approach can become inadequate if the input filter capacitor is oversized with respect to the rated load power or if the load working cycle frequently requires low power level operations. In the latter case, a dynamic compensation by means of equation (4.26) is possible only if the required output to input voltage ratio is also low.

In Fig.4.16, the effect of the not zero reference input current vector phase displacement is shown by the lower, compared to the Fig.4.15 one, minimum instantaneous value of the input line-to-line voltage applied to the output. But the overmodulation operating region is not entered, as it is shown by the output line current waveform in Fig.4.18, because the required output voltage is quite far from the maximum limit, in the case $\frac{\sqrt{3}}{2}\cos 15° \cong 0.836$.

4.5.2 Experimental setup of a Matrix Converter prototype

The three modulation strategies have been implemented on a 7 kVA matrix converter prototype during a six month working period with the Institute of Energy Technology at the university of Aalborg. The block diagram of the prototype setup can be seen in Fig.4.19.

The AC mains is provided by an AC Power Source (15003iX California Instruments) which allows to generate whatever supply voltages condition and to settle the value of the AC mains impedance.

The input filter is given by a second order LC filter. It is used to reduce the input line current ripple and it consists of three series connected inductors (1.2 mH) and three shunt star-connected capacitors (6 μF). In order to better decouple the input side of the matrix converter from the input line inductance, the 6 μF capacitance are splitted in three group of 2 μF per each phase. In this way the input lines are decoupled at each power module input. The input filter,

designed accordingly to the methodology proposed in [23]-[24], has a resonant frequency of 1.876 kHz and gives an attenuation of (YYY dB a 4 kHz da vedere con PSPICE).

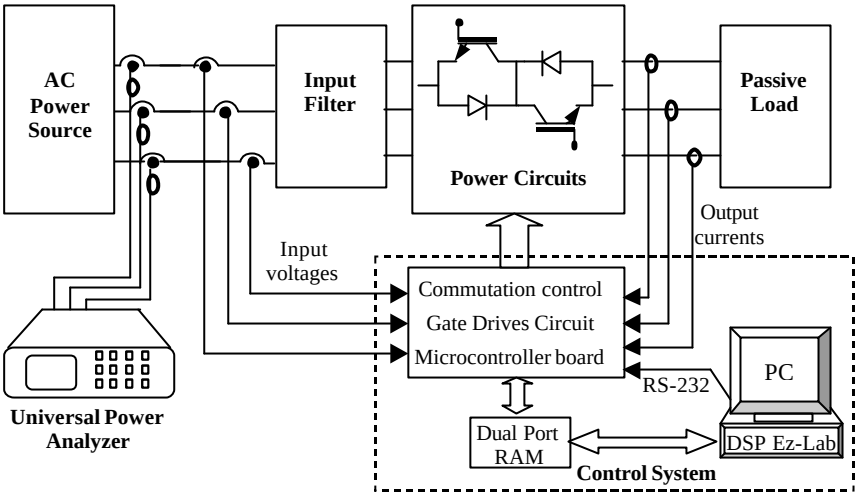

Fig.4.19 Block diagram of the laboratory setup.

The power stage of the matrix converter is based upon three special designed power modules, realized with 1200V, 25A IGBT's and fast recovery diodes. Each module contains three AC switches and each AC switch consists of two anti-paralleled IGBT's in common collector configuration with series diode. A single common clamp circuit protects the converter on the input and on the output side [6], [7]. With regard to the clamp circuit it has to be noted that it does not appear in the mathematical model of Fig.4.10. But the influence of the clamp circuit during normal operation can be considered negligible since the focus of the analysis is pointed to low order harmonic spectra of the input voltages and currents.

The load consists of a three phase star-connrected R-L load.

The control system of the converter is constituted by a dual processors board made up by a floating-point 32/40 bit digital signal processor (DSP) SHARC 21602 from Analog Device and a fixed-point 16 bit microcontroller (µC) SAB80C167 from Siemens. This dual processors solution provides a highly flexible tool for testing of control strategies for power electronics converters and AC drives.

The DSP provides intensive and fast calculation capability, it is interfaced to the host computer and most of all it is provided with a C-compiler which allows to develop the control software using C language instead of assembler. This last feature is a powerful means for boosting control system development.

The µC provides advanced timing functions, as the DSP cycle period and the A/D sampling instant, and it is used for generating the SVM pulses pattern. It has the capability to interface to the host computer too.

The DSP and the μC communicate in the system by way of a dual port RAM. A standard PC provides the user with an interface to the DSP and the μC.

The commutation of the bi-directional switches is managed accordingly to a four step commutation strategy based on the detection of the output current sign. The commuation strategy is implemented of a programmable logic device, one per output phase. Finally, with regard to the control algorithm, for each modulation strategies a simple constant V/f control of the output voltage vector was implemented and a double sided configurations switching sequence was used.

4.5.3 Sinusoidal and unbalanced supply voltages

The equations shown in the following analysis are derived under the assumption that the AC mains impedance and the input filter inductance do not significantly affect the low order harmonic spectrum of the AC mains supply voltages, that is the supply voltages as well as the matrix converter input line-to-neutral voltage vector is assumed to be defined by $\overline{e}_i$.

As aforementioned, in the case of unbalanced sinusoidal supply voltages, only the positive and negative sequence symmetrical components are present in the line-to-neutral voltage vector. Then, the voltage vector $\overline{e}_i$ can be written as

$$\overline{e}_i = \overline{E}_{i_1}\, e^{j\omega_i t} + \overline{E}_{i_{-1}}\, e^{-j\omega_i t} \tag{4.53}$$

The presence of the negative sequence fundamental component cause variations in both magnitude and angular velocity of the input voltage vector whose locus described on the Gauss plane is an ellipse, as shown at the beginning of the chapter in Fig.4.1.b.

In this case, accordingly to equations (4.34) and (4.38), the input voltage disturbance is represented by the negative sequence fundamental component, that is

$$D\,\overline{e}_i = \overline{E}_{i_{-1}}\, e^{-j\omega_i t} \tag{4.54}$$

In Table IV it is shown how the modulation vector $\overline{\psi}$ and the input current vector $\overline{i}_i$ translate for the three strategies.

The unbalanced condition which has been considered for the supply line-to-neutral voltages is defined by the following time phasors

$$\overline{E}_{i_1} = 300V,\ \angle 0^o \qquad \overline{E}_{i_{-1}} = 30\,V,\ \angle 0^o \qquad \text{thereof} \qquad u = \frac{\left|\overline{E}_{i_{-1}}\right|}{\left|\overline{E}_{i_1}\right|} = 0.1 \tag{4.55}$$

where u is defined as the input voltage unbalance degree.

Table IV

Expressions of the modulation and input current vectors for the three strategies. Unbalance.

Strategy A	$\overline{\psi} = \overline{E}_{i\,1}\, e^{j\,\omega_i\, t} + \overline{E}_{i_{-1}}\, e^{-\,j\,\omega_i\, t}$, $\bar{i}_i = \frac{2P_o}{3\overline{E}^*_{i\,1}} e^{\,j\omega_i t} - \frac{2P_o}{3\overline{E}^*_{i_1}} \frac{\overline{E}_{i_{-1}}}{\overline{E}^*_{i_1}} e^{\,j\,3\omega_i t}$
Strategy B	$\overline{\psi} = \overline{E}_{i\,1}\, e^{j\,\omega_i\, t} - \overline{E}_{i_{-1}}\, e^{-\,j\,\omega_i\, t}$, $\bar{i}_i = \frac{2P_o}{3\overline{E}^*_{i\,1}} e^{\,j\omega_i t} - \frac{2P_o}{3\overline{E}^*_{i_1}} \frac{\overline{E}_{i_{-1}}}{\overline{E}_{i_1}} e^{-\,j\,\omega_i t}$
Strategy C	$\overline{\psi} = \overline{E}_{i\,1}\, e^{j\,\omega_i\, t}$, $\bar{i}_i = \frac{2P_o}{3\overline{E}^*_{i\,1}} e^{\,j\omega_i t} - \frac{P_o}{3\overline{E}^*_{i_1}} \frac{\overline{E}_{i_{-1}}}{\overline{E}_{i_1}} e^{-\,j\,\omega_i t} - \frac{P_o}{3\overline{E}^*_{i_1}} \frac{\overline{E}_{i_{-1}}}{\overline{E}_{i_1}} e^{\,j\,3\omega_i t}$

The frequency of the input voltages is 50 Hz. The matrix converter has been controlled in order to generate a three-phase system of balanced line-to-neutral voltages with a maximum amplitude of 132.5 V, which corresponds to an output-to-input voltage ratio equal to 0.43, and a frequency of 25 Hz. The switching frequency is 4 kHz.

Numerical results

In Table V the values of the system parameters relevant to the following numerical simulation results are quoted.

Table V.

System parameters value used by simulations under unbalanced conditions.

L_S [mH]	R_S [Ω]	R_F [Ω]	L_F [mH]	C_F [μF]	L_L [mH]	R_L [Ω]
0.277	0.74	∝	1.2	6	27	15

In Fig.4.20 the unbalanced and sinusoidal supply line-to-neutral voltages correspondent to definition (4.55)are shown.

Figs.4.21-4.26 show the input and output line currents waveforms for the three strategies. In Figs.4.27-4.32 the harmonic spectra of the input line currents and relevant complex space vector are shown for the three strategies.

As it can be seen by Figs.4.21-4.23-4.25, the input line-to-neutral voltages do not differentiate for the three strategies. Consequently, the effect of the input filter capacitance currents can be considered as invariant for the three strategies and almost negligible with respect to the active power delivered to the load. On the basis of these considerations, the following remarks on the input line currents harmonic spectra will be referred to the expressions of the matrix converter input current vector $\bar{i}_i$.

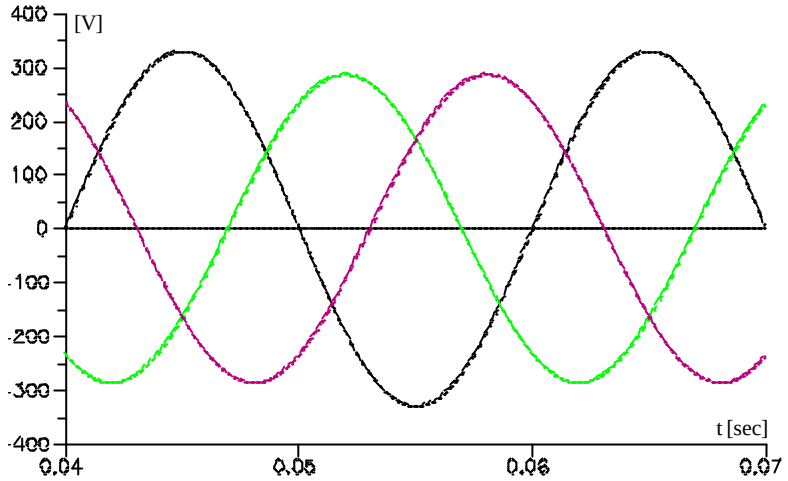

Fig.4.20 Sinusoidal line-to-neutral supply voltages for u=0.1.

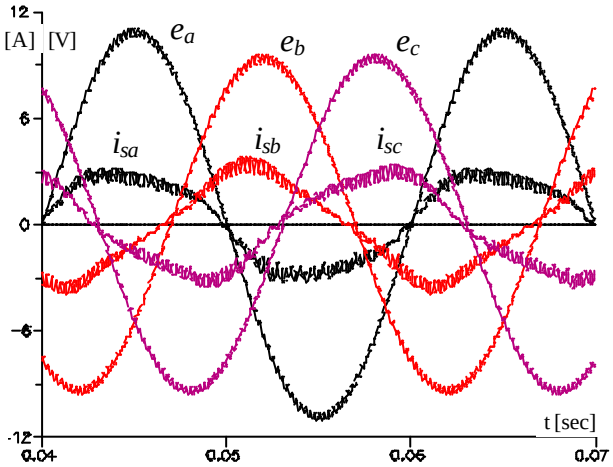

Fig.4.21 Matrix converter input line-to-neutral voltages and line currents. 30V/div. Strategy A.

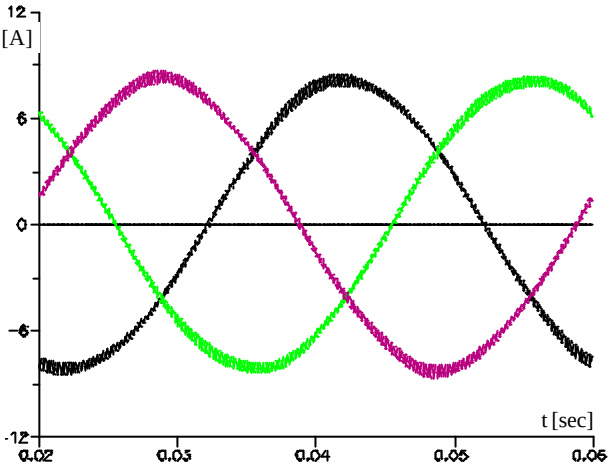

Fig.4.22 Matrix converter output line currents. Strategy A.

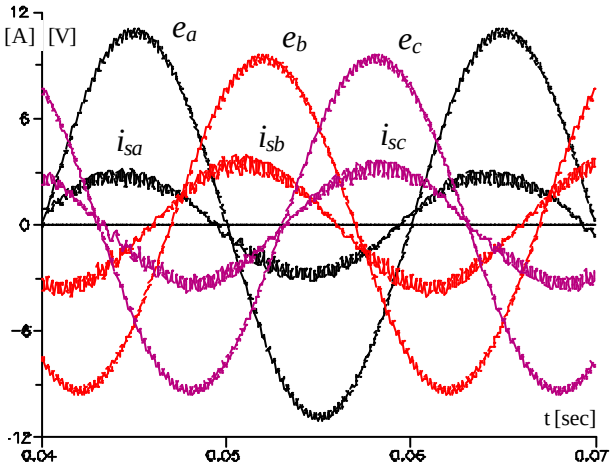

Fig.4.23 Matrix converter input line-to-neutral voltages and line currents. 30V/div. Strategy B.

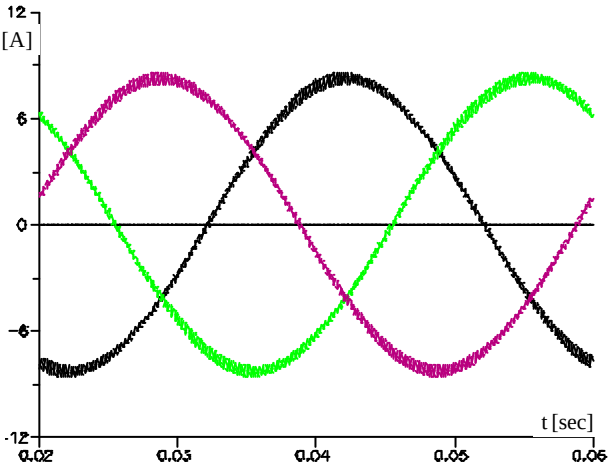

Fig.4.24 Matrix converter output line currents. Strategy B.

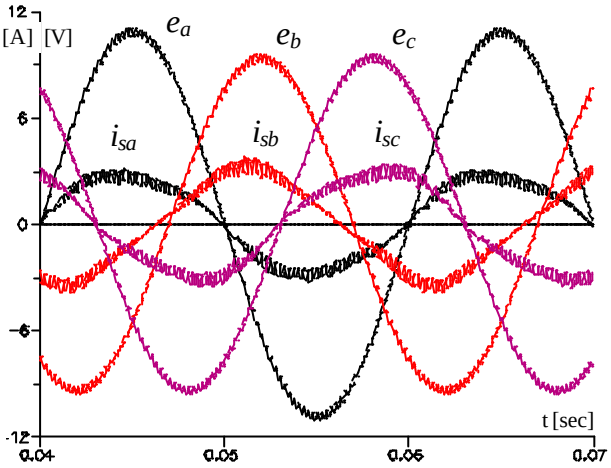

Fig.4.25 Matrix converter input line-to-neutral voltages and line currents. 30V/div. Strategy C.

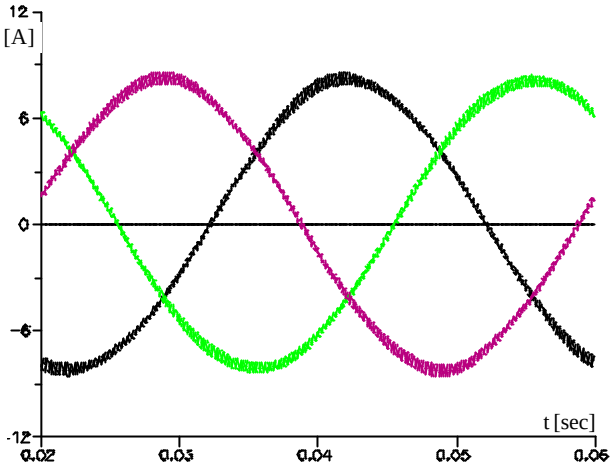

Fig.4.26 Matrix converter output line currents. Strategy C.

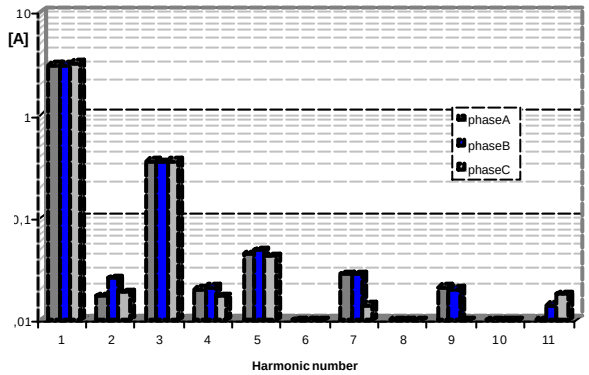

Fig.4.27 Harmonic spectra of input line currents. Strategy A.

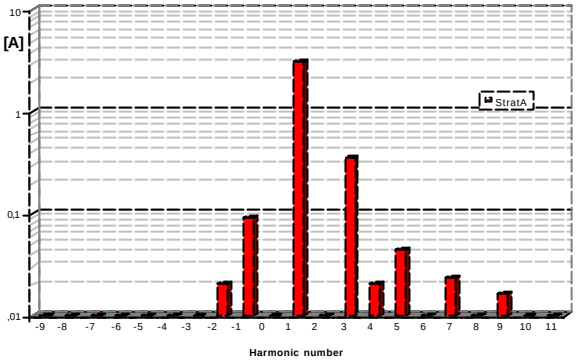

Fig.4.28 Complex harmonic spectrum of the the input line current vector. Strategy A.

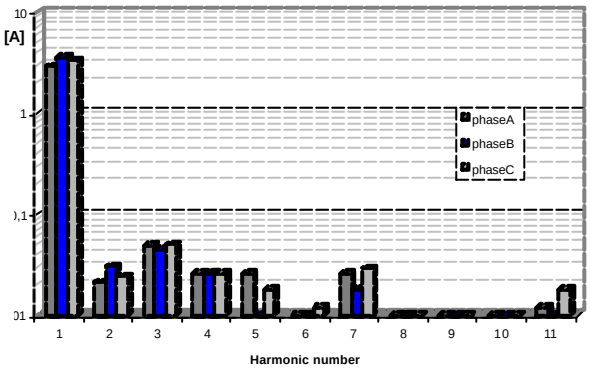

Fig.4.29 Harmonic spectra of input line currents. Strategy B.

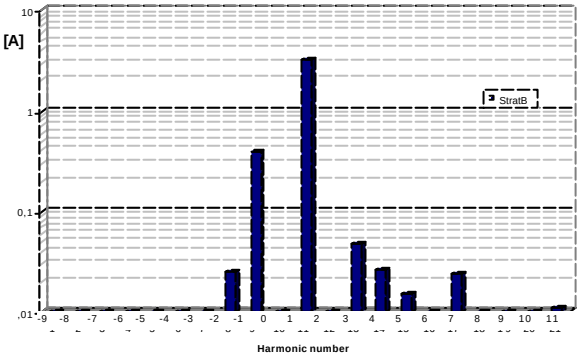

Fig.4.30 Complex harmonic spectrum of the the input line current vector. Strategy B.

With regard to the input line currents it can be noted that for strategy B the waveforms are, as expected, sinusoidal and unbalanced. This is in accord with the input current vector expression quoted in Table IV, where the disturbance is given by only the negative sequence fundamental component. The unbalance of the currents is evident by the different amplitude of the three currents, which can be better appreciated looking at the fundamental components in Fig.4.29.

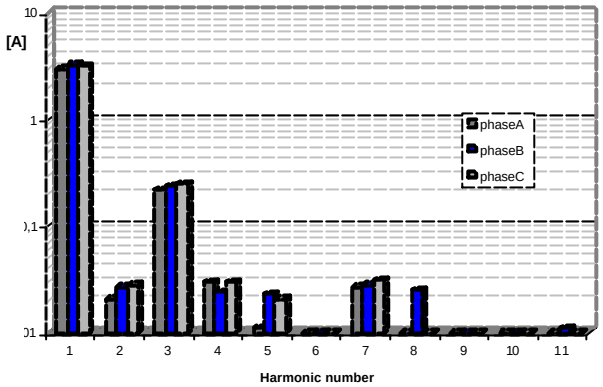

Fig.4.31 Harmonic spectra of input line currents. Strategy C.

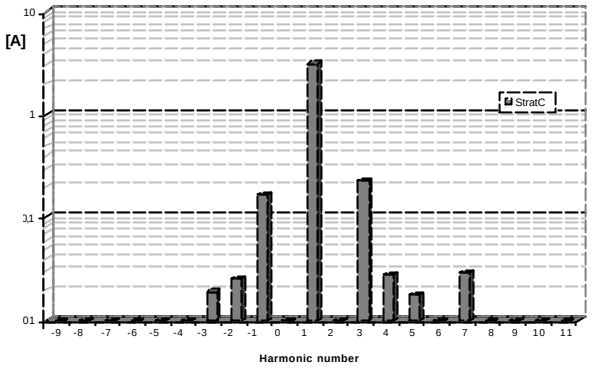

Fig.4.32 Complex harmonic spectrum of the the input line current vector. Strategy C.

It is also worth noting that the phase displacement of the three line currents with respect to the corresponding voltage are different. This result is consistent to the strategy B definition of the modulation vector $\bar{\psi}$, given in Table IV, which establishes that the input current vector is not modulated to be instantaneously in phase with the input voltage vector $\bar{e}_i$ unlikely from strategy A.

In fact, as it can be seen from Fig.4.21, strategy A operates in order to keep, at any instant, the vector $\bar{i}_i$ in phase with the input voltage vector $\bar{e}_i$. Accordingly to the expression in Table IV, the input voltage unbalance degree translates in a proportional input currents harmonic distortion, basically represented by a third harmonic component, as shown in Fig.4.27 and stated by the $\bar{i}_i$ expression inTable IV.

As far as the strategy C is concerned it has an intermediate behavior between strategy A and B. It can be seen from Fig.4.25 and verified by the input current vector $\bar{i}_i$ expression inTable IV that the input line currents are both distorted by a third harmonic as in strategy A and unbalanced as in strategy B, but to a smaller extent. The reduction of these input current disturbances is shown in Fig.4.31, where the amplitude difference of the fundamental input line currents component is lower compared to strategy B and the third harmonic component amplitude is nearly halved with respect to strategy A.

With regard to the output voltage performance it is important to highlight that, as shown by Fig.4.22, 4.24, 4.26, all strategies are capable of maintaining balanced and sinusoidal output voltages even with unbalanced input voltages.

In Table VI the performance of the three strategies in terms of input current quality are quoted with regard to the input current vector. These RMS values have been calculated using equations (4.40) and (4.41) and taking into account the first 11 positive and negative harmonic components of the input line current space vector.

It can be seen that, accordingly to [19] strategy A provides the lowest RMS value of the three phase input line current system, but strategy C is the better performing in terms of minimization of the input current disturbance RMS value.

Table VI.
Input line current quality performance. Unbalance.

	Strategy A	Strategy B	Strategy C
$I_{3_{RMS}}$ [A]	3.82	4.01	3.84
$Di_{i_{RMS}}$ [A]	0.37	0.39	0.29

Experimental results

As aforementioned, the three modulation strategies have been implemented of a 7 kVA matrix converter prototype and their performance have been tested under sinusoidal and unbalanced input voltage conditions. The experimental results shown in this section relate to a comparison of strategy A and strategy B [25].

In this case the passive load parameters were R_L = 12Ω and L_L = 0.027H for a correspondent total active power delivered to the load of approximately 1.9 kW. This is the only difference with respect to the system and control parameters value used for the previous numerical simulation results.

The harmonic components of the three input line currents were measured using a universal power analyzer PM3000A fromVoltech.

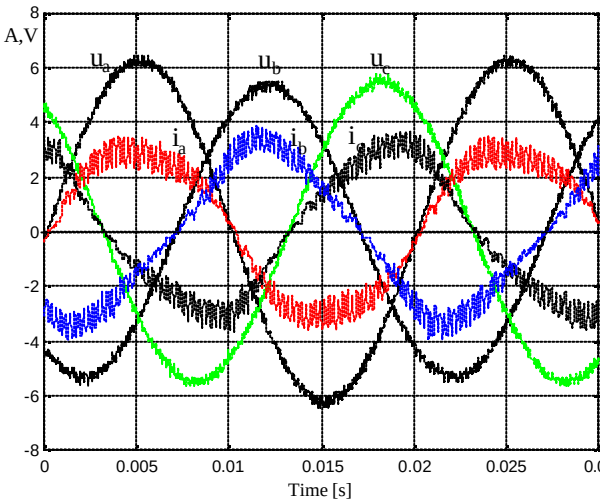

Fig.4.33 Matrix converter input line-to-neutral voltages and line currents. Strategy A. 100V/div and 2.5A/div.

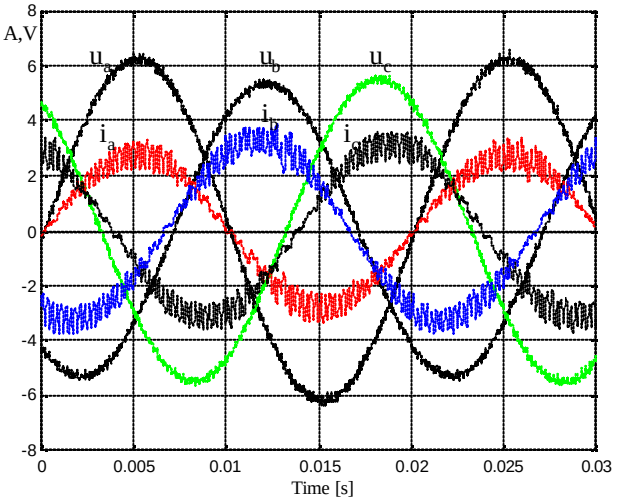

Fig.4.34 Matrix converter input line-to-neutral voltages and line currents. Strategy B. 100V/div and 2.5A/div.

Looking at Figs.4.33-4.36, it can be stated that the experimental results are in good accordance with the numerical ones. In Figs.4.37 and 4.38 the harmonic spectra of input line currents i_{sa} and i_{sb} are compared for the two strategies. It is evident the cancellation of the third harmonic component carried out by strategy B. The same holds for current i_{sc} obviously. With

regard to strategy A it is also worth noting that the third harmonic to fundamental amplitude ratio is nearly equal to the input voltages unbalanced degree, u = 0.1, as predicted by the linearized analysis (Table IV).

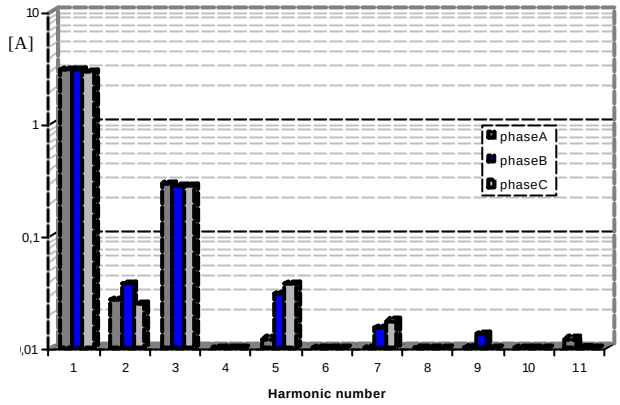

Fig.4.35 Harmonic spectra of input line currents. Strategy A.

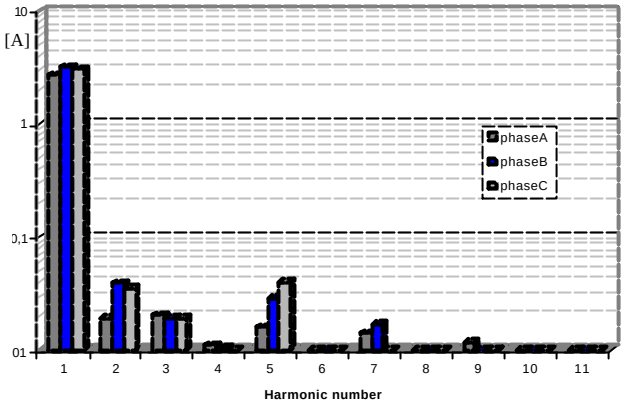

Fig.4.36 Harmonic spectra of input line currents. Strategy B.

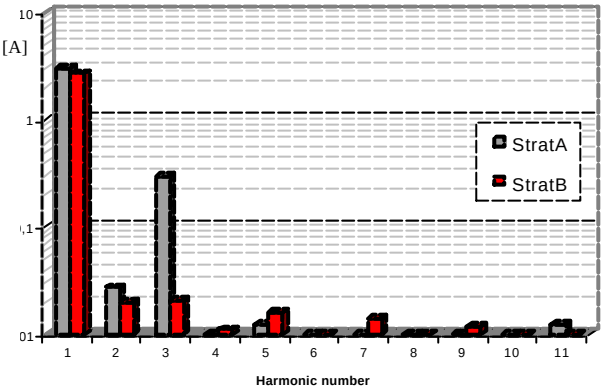

Fig.4.37 Harmonic spectra of input line current i_a. Strategy A and B.

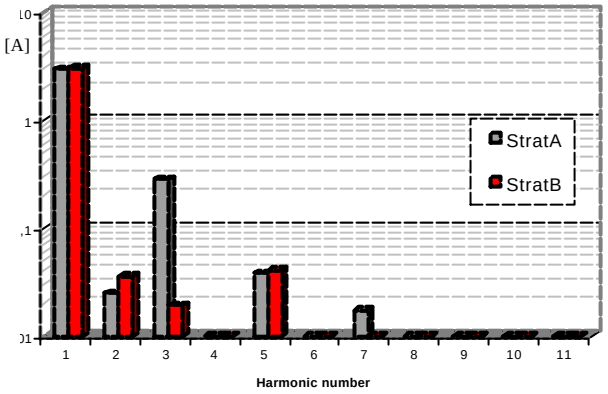

Fig.4.38 Harmonic spectra of input line current i_b. Strategy A and B.

In Table VII the data collected during the experimental measurements are quoted. Some comments can be made.

Table VII.
Measurement data.

	Strategy A			Strategy B		
Quantity	Phase a	Phase b	Phase c	Phase a	Phase b	Phase c
Voltage (V)	232.5	201.6	201.7	232.5	201.6	201.7
Line Current RMS (A)	3.08	3.07	3.00	2.81	3.09	3.28
Active Power (W)	708	612	593	628	640	607
Reactive Power (Var)	134	116	115	104	140	142
Apparent Power (VA)	720	624	603	637	655	624
Power Factor	0.983	0.982	0.981	0.986	0.976	0.973
THD_v %	1.3	1.3	1.1	1.1	1.5	1.5
THD_i %	17.7	16.8	17.	15.0	13.9	13.9
HD_{11} %	9.7	9.8	9.5	1.5	1.9	1.8
Three Phase $I_{3_{RMS}}$ (A)	5.28			5.3		

Looking at the power factor and line current amplitude values it is confirmed that strategy B determines an unbalance in the input line currents. For strategy A the input line currents system is nearly balanced: the current RMS values for the three phases are nearly the same. The power factor is not as close to unity as it would be expected because of the current drawn by the input filter capacitance, which determines a slight leading displacement of the input line current.

As far as the input power quality is concerned it has to be highlighted the significant reduction of the low order current harmonic components carried out by strategy B compared to strategy A as shown in Table VII by the distortion factor HD_{11}. Considering the line current total harmonic distortion factor THD_i, the improvements obtained by strategy B are still significant but to a smaller extent. This is due to the relevant amplitude of the switching harmonic components whose squared value is taken into account by the power analyzer for calculating the THD_i.

Looking at Table VII, strategy B compared to strategy A determines a slightly higher three phase RMS value for the input line currents as shown by I_{3RMS}. This result is in accord with the theoretical analysis which would expect for strategy A the minimum three phase RMS value for the input line currents.

In Figs.4.39 and 4.40 the experimental loci of the input line current and line-to-neutral voltage vectors for strategy A and strategy B are shown. The current locus for strategy B is a pure ellipse whereas for strategy A the shape is distorted, basically from the third harmonic component.

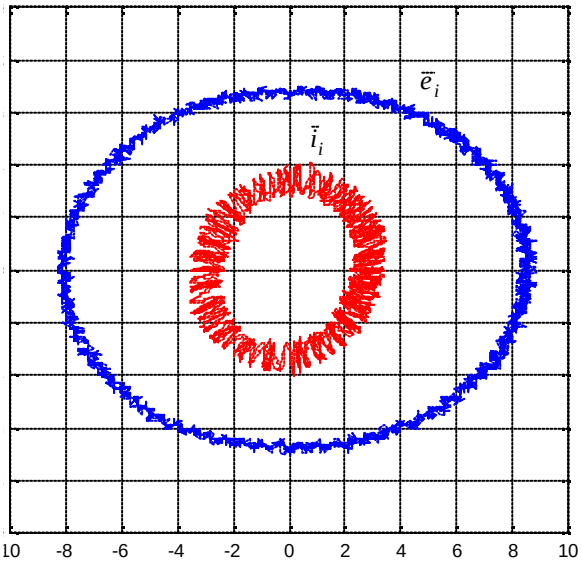

Fig.4.39 Input line current and line-to-neutral voltage vectors loci for strategy A.
80V/div and 2.5A/div

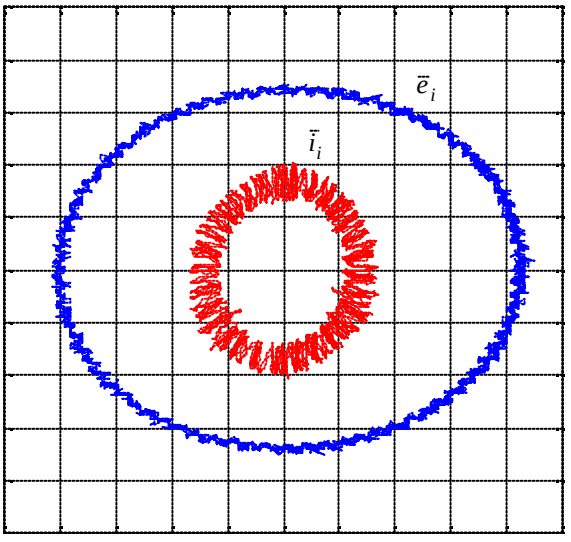

Fig.4.0 Input line current and line-to-neutral voltage vectors loci for strategy B.
80V/div and 2.5A/div.

4.5.4 Nonsinusoidal and balanced supply voltages

As for to the previous case of unbalance, even when the supply voltages are nonsinusoidal and balanced, both magnitude and angular velocity of the input voltage vector $\overline{e}_i$ vary due to the presence of the harmonic components. The operating condition that has been considered is defined by the following time phasors

$$\overline{E}_{i_1} = 300V,\ \angle 0^o \qquad \overline{E}_{i_{+7}} = 15V,\ \angle 0^o \qquad \overline{E}_{i_{-11}} = 9V,\ \angle 0^o \tag{4.54}$$

As a consequence, the matrix converter input line-to-neutral voltage vector $\overline{e}_i$ and the input voltage disturbance vector $D\overline{e}_i$ are respectively given by

$$\overline{e}_i = \overline{E}_{i_1} e^{j\omega_i t} + \overline{E}_{i_{+7}} e^{j7\omega_i t} + \overline{E}_{i_{-11}} e^{-j11\omega_i t} \tag{4.55}$$

$$D\overline{e}_i = \overline{E}_{i_{+7}} e^{j7\omega_i t} + \overline{E}_{i_{-11}} e^{-j11\omega_i t} \tag{4.56}$$

In the same way as for the unbalance case, it is possible to define for any harmonic component of the input voltage vector a distortion degree d . In the case the distortion degrees are given by

$$d_{+7} = \frac{\left|\overline{E}_{i_{+7}}\right|}{\left|\overline{E}_{i_1}\right|} = 0.05 \quad , \quad d_{-11} = \frac{\left|\overline{E}_{i_{-11}}\right|}{\left|\overline{E}_{i_1}\right|} = 0.03 \tag{4.57}$$

Table VIII.
Expressions of the modulation and input current vectors for the three strategies. Distortion

Strategy A	$\overline{\psi} = \overline{e}_i$ $\overline{i}_i = \frac{2P_o}{3\overline{E}_{i_1}^*} e^{j\omega_i t} - \frac{2P_o}{3\overline{E}_{i_1}^*} \frac{\overline{E}_{i_{+7}}}{\overline{E}_{i_1}} e^{-j5\omega_i t} - \frac{2P_o}{3\overline{E}_{i_1}^*} \frac{\overline{E}_{i_{-11}}}{\overline{E}_{i_1}} e^{+j13\omega_i t}$
Strategy B	$\overline{\psi} = \overline{E}_{i_1} e^{j\omega_i t} - \overline{E}_{i_{+7}} e^{j7\omega_i t} - \overline{E}_{i_{-11}} e^{-j11\omega_i t}$ $\overline{i}_i = \frac{2P_o}{3\overline{E}_{i_1}^*} e^{j\omega_i t} - \frac{2P_o}{3\overline{E}_{i_1}^*} \frac{\overline{E}_{i_{+7}}}{\overline{E}_{i_1}} e^{+j7\omega_i t} - \frac{2P_o}{3\overline{E}_{i_1}^*} \frac{\overline{E}_{i_{-11}}}{\overline{E}_{i_1}} e^{-j11\omega_i t}$
Strategy C	$\overline{\psi} = \overline{E}_{i_1} e^{j\omega_i t}$ $\overline{i}_i = \frac{2P_o}{3\overline{E}_{i_1}^*} e^{j\omega_i t} - \frac{P_o}{3\overline{E}_{i_1}^*} \frac{\overline{E}_{i_{+7}}}{\overline{E}_{i_1}} e^{-j5\omega_i t} - \frac{P_o}{3\overline{E}_{i_1}^*} \frac{\overline{E}_{i_{+7}}}{\overline{E}_{i_1}} e^{j7\omega_i t} - \frac{P_o}{3\overline{E}_{i_1}^*} \frac{\overline{E}_{i_{-11}}}{\overline{E}_{i_1}} e^{-j11\omega_i t} - \frac{P_o}{3\overline{E}_{i_1}^*} \frac{\overline{E}_{i_{-11}}}{\overline{E}_{i_1}} e^{j13\omega_i t}$

In Table VIII it is shown how the modulation vector $\bar{\psi}$ and the input current vector $\bar{i}_i$ general expressions translate for the three strategies. As for Table IV, the equations assume that the supply impedance and the input filter do not significantly affect the low order harmonic spectrum of the AC mains supply voltages, therefore $\bar{e}_i$ can be considered the AC mains supply voltage vector as well as the matrix converter input line-to-neutral voltage vector.

As in the previous case the frequency of the input voltages is 50 Hz. The matrix converter has been controlled in order to generate a system of balanced line-to-neutral voltages with a maximum amplitude of 132.5 V and a frequency of 25 Hz. The switching frequency is 4 kHz.

Numerical results

The values of the system parameters related to the following numerical simulation results are still those quoted in Table V. In Fig.4.41 the balanced and nonsinusoidal supply voltages for the operating condition defined by (4.54) are shown.

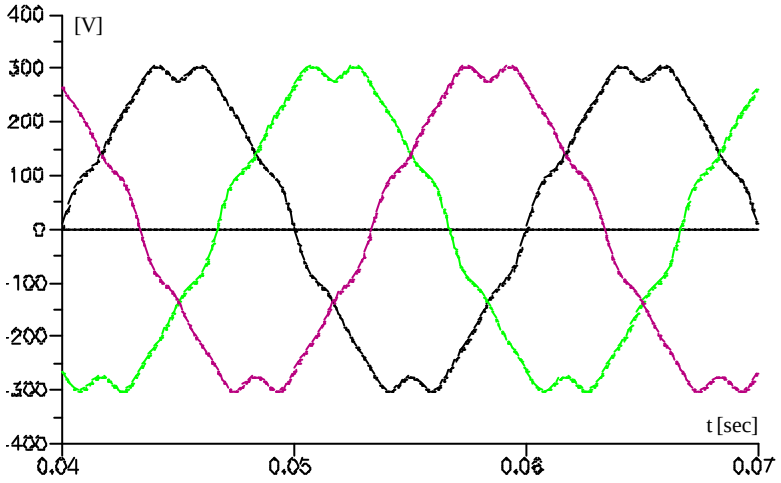

Fig.4.41 Nonsinusoidal and balanced line-to-neutral supply voltages.

Figs.4.42-4.27 show the input and output line currents waveforms for the three strategies.

As it can be seen by Figs.4.42-4.44-4.46, the input line-to-neutral voltages do not differentiate for the three strategies. Consequently, the effect of the input filter capacitance currents can be considered as invariant for the three strategies and almost negligible, in terms of input line current phase displacement, due to the active power delivered to the load.

But in this case, the input filter capacitance current has the effect to conceal the performance of the three strategies. Two are the reasons basically.

The first is that any matrix converter modulation strategy exerts its control capability only on the input line current component which is fed to the output load, but it has no control of the input filter capacitance current.

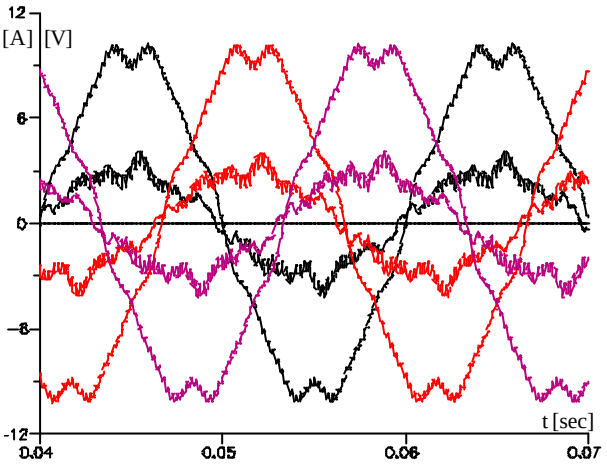

Fig.4.42 Matrix converter input line-to-neutral voltages and line currents. 30V/div. Strategy A.

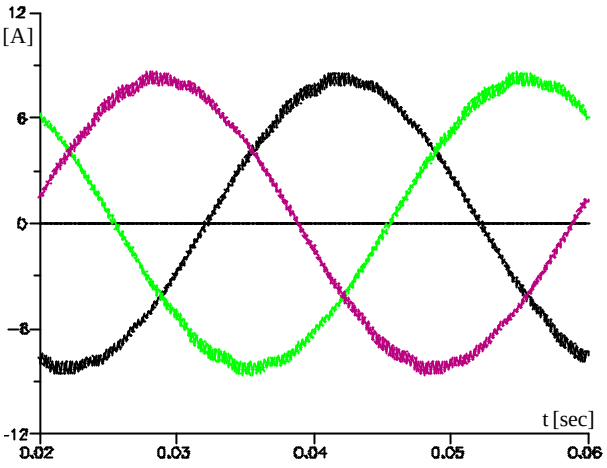

Fig.4.43 Matrix converter output line currents. Strategy A.

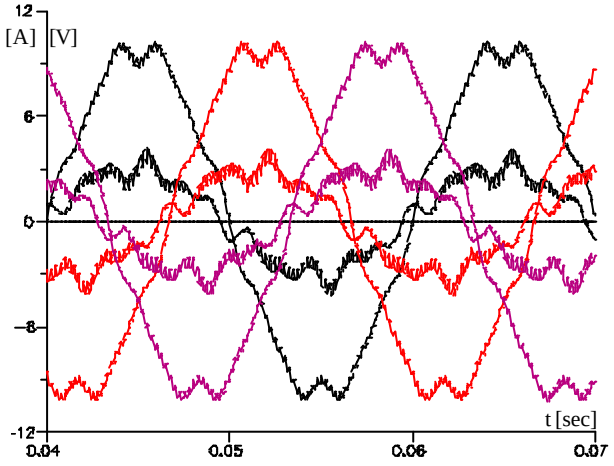

Fig.4.44 Matrix converter input line-to-neutral voltages and line currents. 30V/div. Strategy B.

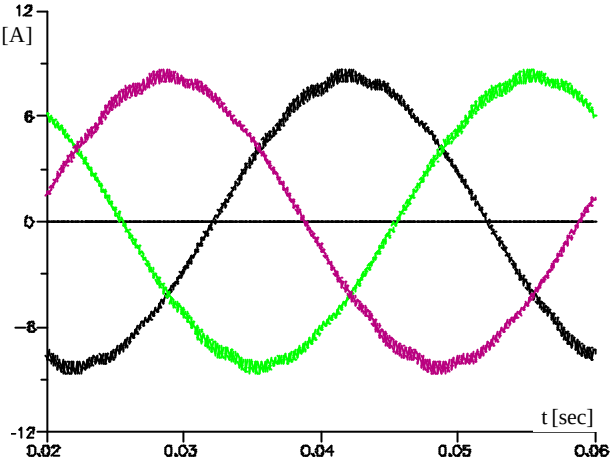

Fig.4.45 Matrix converter output line currents. Strategy B.

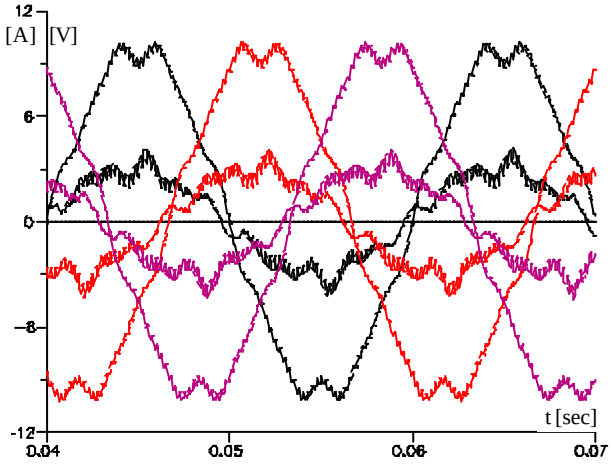

Fig.4.46 Matrix converter input line-to-neutral voltages and line currents. 30V/div. Strategy C.

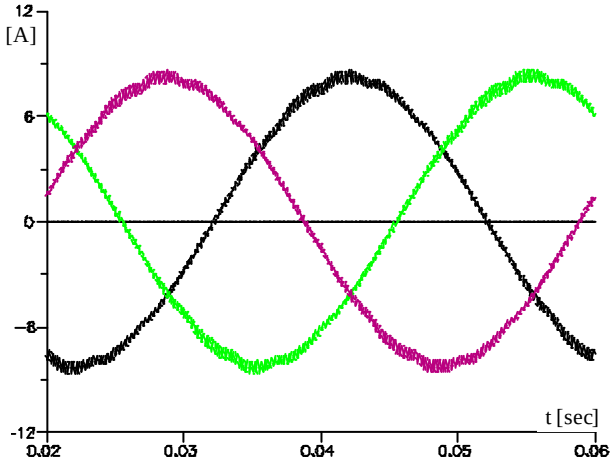

Fig.4.47 Matrix converter output line currents. Strategy C.

The second is that any voltage harmonic component which is present on the grid produces an equal order current harmonic component to be drawn by the filter capacitors. The percentage of such harmonic component in the line current spectrum decreases when the converter input current increases, that is when the power to the load rises. On the contrary, the current harmonic components introduced by the modulation strategies maintain an approximately constant relative amplitude.

With respect to the operating condition here considered for both simulations and experimental tests, although the power delivered to the load is sufficient to assume almost negligible the effect of the input filter current on the power factor, it is not sufficient to allow a clear analysis of the performance of the three strategies.

Therefore, the figures of the harmonic spectra shown hereinafter will be referred to the matrix converter input current. Moreover, on the basis of the calculated harmonic spectra, which have shown that the fundamental component value of the input line currents does not change for the three strategies (differences are in the range of ± 0.3 % ≅ 10 mA) the scale of the y axis is set linear and limited to 10% of the fundamental component amplitude.

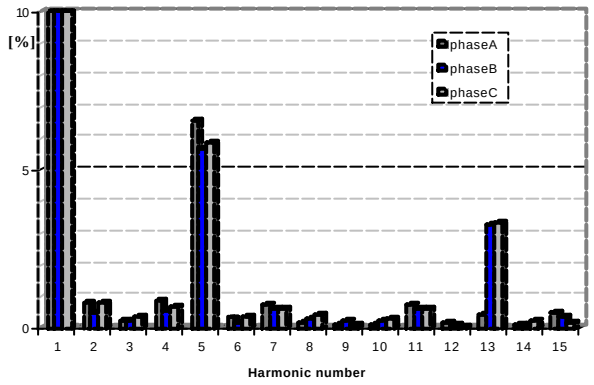

Fig.4.48 Harmonic spectra of matrix converter input currents. Strategy A.

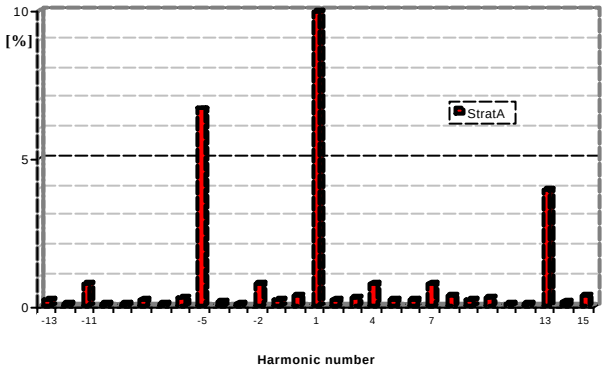

Fig.4.49 Complex harmonic spectrum of the input current vector. Strategy A.

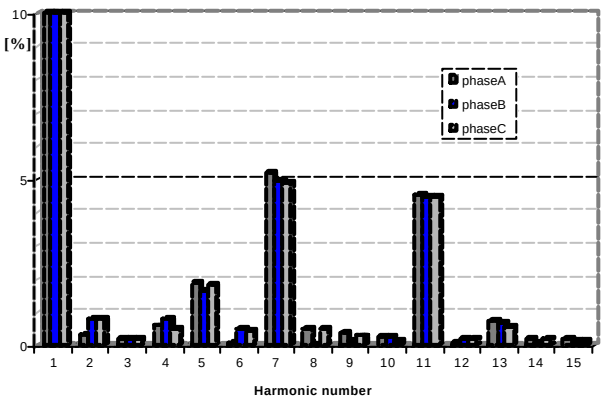

Fig.4.50 Harmonic spectra of matrix converter input currents. Strategy B.

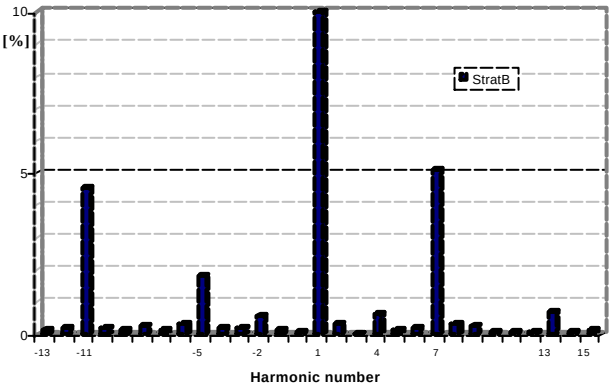

Fig.4.51 Complex harmonic spectrum of the input current vector. Strategy B.

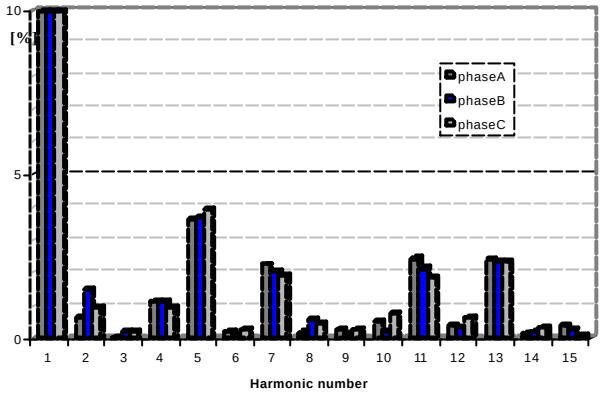

Fig.4.52 Harmonic spectra of matrix converter input currents. Strategy C.

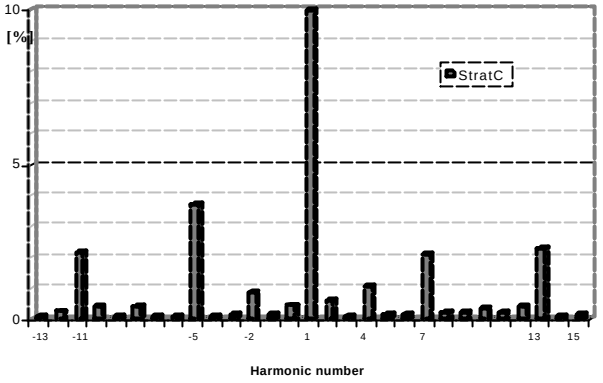

Fig.4.53 Complex harmonic spectrum of the input current vector. Strategy C.

Looking at Figs.4.42-4.44-4.46 it can be seen that the input line currents are no longer unbalanced but the waveforms are significantly distorted. In Figs.4.43-4.45-4.47 the output line currents are shown. It is evident that, even under distorted input voltages conditions the three modulation strategies are capable of maintaining balanced and sinusoidal output voltages.

In Figs.4.48-4.49 the harmonic spectra of the matrix converter input currents and relevant vector are respectively shown for strategy A. In good accord with the input current vector expression given in Table VII, vector $\bar{i}_i$ presents a negative sequence harmonic component of order k = -5 whose amplitude is proportional to the distortion degree d_{+7} and a positive sequence harmonic component of order k = +13 whose amplitude is proportional to the distortion degree d_{-11}, as it can be seen in Fig.4.49.

In the case of strategy B the harmonic spectra still meet the linearized analysis expectation. In particular, the harmonic components have the same order of the input voltage harmonics and the magnitude is proportional to the relevant distortion degree. However, comparing the spectra of the two strategies, it can be noted that the "amount of distortion" does not change significantly, as the current harmonic components are just swept to different harmonic order.

With strategy C the harmonic spectra change. The effect of each input voltage harmonic component is splitted onto different current harmonic orders which have a magnitude that is proportional to half of the distortion degree value of the input voltage harmonic component in object. The effect, as stated above, is a reduction of the total RMS value of the input current low order harmonic content with consequent improvement of the input current total harmonic distortion.

In Table IX the performance of the three strategies in terms of input current quality are quoted. In this case, the RMS values have been calculated taking into account the first 15 positive and negative harmonic components of the input current space vector. It can be noted that strategy C still provides the best performance with respect to RMS value of the input current disturbance while strategy A give the lowest three phase RMS value.

Table IX.
Matrix converter input current quality performance. Distortion.

	Strategy A	Strategy B	Strategy C
I_{3RMS} [A]	3.27	3.27	3.28
$Di_{i_{RMS}}$ [A]	0.248	0.234	0.185

Experimental results

Under the nonsinusoidal and balanced supply voltages condition defined accordingly to (4.54) strategies A and C have been experimentally tested and compared. The values of the load resistance and inductance was set to 13 Ω and 27 mH respectively. The frequency of the input voltages is 50 Hz. The matrix converter has been controlled in order to generate a three-phase system of balanced line-to-neutral voltages with a maximum amplitude of 132.5 V and a frequency of 25 Hz. The switching frequency is 4 kHz.

The harmonic components of the three input currents have been measured using a universal Power Analyzer PM3000A from Voltech. A TDS3014 Oscilloscope and a AM503 Current Probe Amplifier from Tektronix have been also used for measurements and currrents harmonic spectrum determination.

For displaying purpose, the scale of the y axis in the harmonic spectra figures is set linear and limited to 10% of the fundamental component amplitude as for the numerical results.

In Fig.4.54 the harmonic spectrum of the input line current i_{sa} is compared for the two strategies. In Table X the corresponding harmonic distortion factor HD_{15} values are quoted. By looking at these figure and data, no significant differences can be appreciated between strategy A and strategy C and the harmonic content is not in accord with the linearized analysis results. The performance of the two strategiesi are hidden by the current drawn by the filter capacitors.

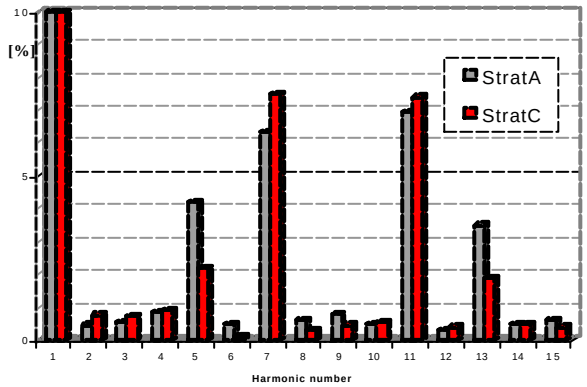

Fig.4.54 Input line current i_{sa} harmonic spectrum comparison.

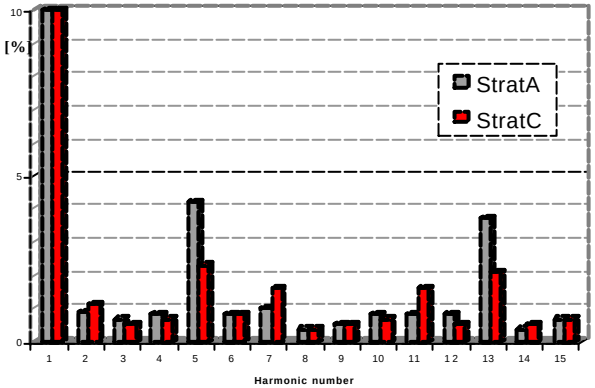

Fig.4.55 Matrix converter input current i_a harmonic spectrum comparison.

Table X.
Harmonic distortion factor HD_{15} of the input line currents. [%]

	line a	line b	line c
strategy A	11.2	11.2	11.2
strategy C	10.9	10.9	10.9

In order to exclude the effect of the input filter capacitor currents from the line current harmonic spectrum and make evident the performance the two strategies, the following three step measurement procedure has been used:

i) the input line current waveform was firstly acquired, by an oscilloscope, with matrix converter not operating;
ii) the input line current waveform was secondly acquired with the matrix converter operating to the settled condition;
iii) the first waveform was subtracted to the second one and a Fourier analysis was performed on the resulting waveform. The waveform acquisitions at point i) and ii) were synchronized to the same input line to neutral voltage.

By means of this procedure it is possible to determine a reliable low order harmonic spectrum of the matrix converter input current.

In Fig.4.55 the harmonic spectrum of the input current i_a is shown for strategies A and C. It can be seen that the harmonic spectra are now consistent with the numerical results as well as linearized analysis expression of the input current vector quoted in Table VIII.

For strategy A only two current harmonic components are evident, those having order 2-k. For strategy C these harmonic components have the amplitude nearly halved and two new harmonic components of k order are introduced.

In Table XI the harmonic distortion factor HD_{15} and the three phase RMS value of the matrix converter input currents system, calculated accordingly to equations (4.51) and (4.52), are quoted.

Table XI.
Harmonic distortion factor and three phase RMS value of the matrix converter input currents

	strategy A			strategy C		
	line a	line b	line c	line a	line b	line c
HD_{15} [%]	6.2	6.2	5.7	4.4	4.6	4
I_{3RMS} [A]	2.9			2.95		

Table XI clearly shows that strategy C brings about a significant reduction of the input current harmonic distortion with respect to strategy A. But strategy A still have the minimum three phase input current RMS value.

It is here important to point out that the results shown in Table XI hold for the input line currents too increasing the power to the load. As the output power delivered to the load is increased as much the effect of the input filter current on the input line current is reduced.

The I_{3RMS} values quoted in Table XI have been calculated on the basis of the first 15 harmonic components of the input current waveforms determined at step iii) of the above measurement procedure. The Blackman-Harris window of the oscilloscope has been used to perform the fast Fourier transform (FFT) of the input currents.

In Fig.4.56 the harmonic spectrum of the input current i_a obtained by means of the oscilloscope FFT utility is shown. The scale on the y axis is linear and limited to 10 % of the fundamental. The scale on the x axis is also linear with 250Hz per division.

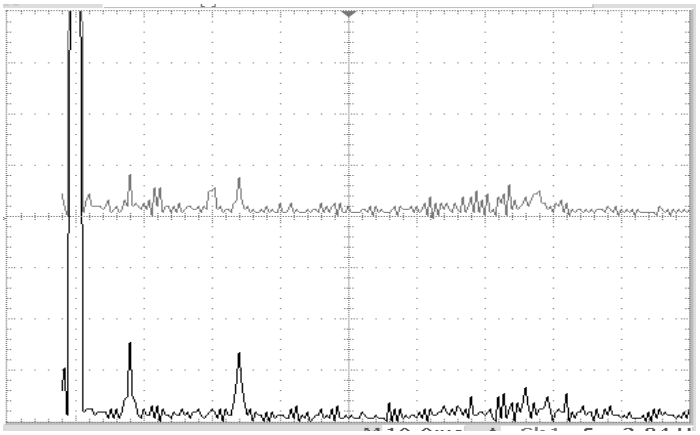

Fig.4.56 Harmonic spectrum of the matrix converter input current i_a by the oscilloscope.2.5 % / div.

In Fig. 4.57 the waveform and the relevant harmonic spectrum of the output currents generated by both strategies are shown. This figure shows that both strategies even under nonsinusoidal supply voltages are able to maintain a balanced and sinusoidal output voltage system. In this case the correspondent currents did not present any harmonic component which exceeds the 0.6% of the fundamental.

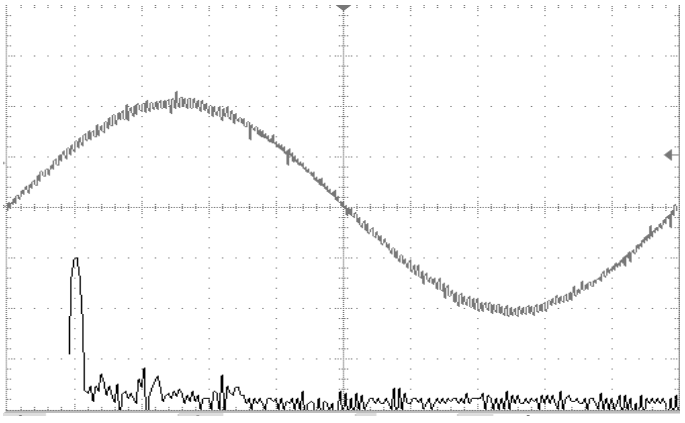

Fig.4.57 Output line current waveform and relevant harmonic spectrum. 20 Hz output frequency. Strategy C.

With regard to the waveform on the y axis the scale is 5A per division; on the x axis is 10ms per division. For the harmonic spectrum, on the y axis the scale is 20dB per division; on the x axis is 250 Hz per division and it is linear.

In Table XII the data measurements collected by the power analyzer are quoted. Looking at the active power it has to be noted that the three phase value, which can be practically viewed as the output power to the load, is basically the same for the two strategies. This is an important data since it verifies one of the basic assumption made by the linearized analysis.

Finally, as expected even the three phase value of the input line current is lower for strategy A.

Table XII.
Measurement data for distortion.

Quantity	Strategy A			Strategy C		
	Phase a	Phase b	Phase c	Phase a	Phase b	Phase c
Voltage (V)	219.2	219.2	219.3	219.1	219.2	219.3
Line Current RMS (A)	2.41	2.4	2.43	2.47	2.45	2.68
Active Power (W)	516	514	518	521	520	522
Reactive Power (Var)	126	113	124	146	134	143
Apparent Power (VA)	642	627	642	667	654	665
Power Factor	0.972	0.976	0.973	0.962	0.968	0.964
THD_v %	6.	6	6	6	6	6
THD_i %	22.3	20.6	22.3	22.1	20.4	22.2
Three Phase I_{3RMS} (A)	4.18			4.39		

4.6 Conclusions

Three modulation strategies for space vector controlled matrix converters have been presented. As the matrix converter has no internal energy storage, disturbances in the input voltages will be coupled directly to the output terminals of the converter. If the input voltages are unbalanced and/or distorted it is necessary to compensate such disturbances in order to maintain balanced and sinusoidal output voltages.

But carrying out this compensation, low order harmonics will be generated in the converter input currents.

The three strategies, A, B, C, differ for the direction along which the input current vector is modulated.

Strategy A operates in order to keep at any instant the input current vector $\bar{i}_i$ in phase with the input line-to-neutral voltage vector $\bar{e}_i$, that means instantaneous unity input power factor.

For strategies B and C the input current vector $\bar{i}_i$ is dynamically modulated along a direction which oscillates around the input voltage vector $\bar{e}_i$. Higher the input voltage disturbance higher the oscillation. Nevertheless , unity input power factor is obtained on the fundamental period average.

On the basis of a linearization of the matrix converter input/output equations the performance of these three strategies have been analysed. The input current quality has been evaluated by the criteria of three phase RMS value (line losses), total RMS value of the input current disturbance and a low order harmonic distortion factor.

Numerical simulations have been firstly carried out to verify the analysis. The three modulation strategies have been then implemented on a matrix converter prototype with the Institute of Energy Technology at the university of Aalborg, Denmark. Tests have been carried out either under unbalanced or distorted supply voltages conditions. The collected results, with respect to the strategies performance, have confirmed the linearized analysis validity showing good accordance with the numerical results.

It is concluded that within the accepted range of unbalance and distortion, strategy C might be preferred to the more straight-forward and commonly implemented strategy A as it provides an appreciable reduction of the input current disturbance RMS value and consequently of the input current harmonic content. Strategy B might be preferred in special condition where highly unbalanced supply voltages exist.

References

[1] L. Gyugyi, B.R. Pelly, "Static Power Frequency Changers. Theory, performance and applications," ISBN 0-471-678000-7, 442 pages, John Wiley & Sons, USA, 1976

[2] M. Venturini, "A new sine wave in, sine wave out, conversion technique eliminates reactive elements," in Proceedings of Powercon 7, San Diego, CA, 1980, pp. E3-1-E3-15.

[3] P.D. Ziogas, S.I. Khan, and M.H. Rashid, "Some Improved Forced Commutated Cycloconverters Structure", IEEE Transactions on Industry Applications, vol. IA-21, No 5, Sept./Oct. 1985, pp. 1242-1253.

[4] P.D. Ziogas, S.I. Khan, and M.H. Rashid, "Analysis and Design of Forced Commutated Cycloconverter Structures with Improved Transfer Characteristics," IEEE Transactions on Industry Applications, vol. IE-33, No. 3, August 1986, pp. 271-280.

[5] C. D. Schauder, "Hidden DC-link AC/AC converter using bilateral power switches," U.S. Patent # 4,642,751, Westinghouse Electric Corporation, February 10,1987.

[6] C.L. Neft and C.D. Schauder, "Theory and Design of a 30-Hp Matrix Converter", Conference Records of IEEE/IAS Annual Meeting, 1988, pp. 934-939.

[7] A. Alesina, M. Venturini, "Intrinsic amplitude limits and optimum design of 9-switches direct PWM ac-ac converters," Proceedings of IEEE/PESC'88, vol. 2, pp. 1284-1291, 1988.

[8] G. Roy, G-E. April, “Cycloconverter operation under a new scalar control algorithm,” Conference Records of IEEE PESC 1989, Milwaukee, WI, June 26-29, 1989, pp. 368-375.

[9] L. Huber, D. Borojevic, “Space Vector Modulator for Forced Commutated Cycloconverters” Proceedings of IEEE/PESC’89, pp. 871-876, 1989.

[10] L. Huber, D. Borojevic, “Space vector modulation with unity input power factor for forced commutated cycloconverters”, in Conference Records of IEEE Industry Applications Society Annual Meeting, 1991, Part I, pp. 1032-1041.

[11] D. Casadei, G. Grandi, G. Serra, A. Tani, “Space vector control of matrix converters with unity input power factor and sinusoidal input/output waveforms,” Proceedings of IEE-EPE'93, Vol. 7, pp. 170-175, 1993.

[12] A.Ferrero and G. Superti-Furga, “A New Approach to the Definition of Power Components in Three-Phase Systems Under Nonsinusoidal Conditions,” IEEE Transactions on Instrumentation and Measurements, vol. 40, no. 3, pp. 568-577, June 1991.

[13] S. Halász, I. Schmidt, T. Molnár, ”Matrix Converters for Induction Motor Drive”, Proceedings of EPE’95, vol. 2, pp. 664-669,1995.

[14] M. Milanovic and B. Dobaj, “A Novel Unity Power Factor Correction Principle in Direct AC to AC Matrix Converters,” Proceedings of IEEE/PESC 1998, pp. 746-752.

[15] D. Casadei, G. Grandi, G. Serra, A. Tani, “Analysis of space vector modulated matrix converter under unbalanced supply voltages”, Proceedings of SPEEDAM'94, Taormina (Italy), 8-10 June, 1994, pp. 39-44.

[16] D. Casadei, G. Serra, A. Tani, P. Nielsen, “Performance of SVM controlled matrix converter with input and output unbalanced conditions”, Proceedings of EPE’95, Vol. II, Sevillle, 18-21 Sept. 1995, pp. 628-633.

[17] D. Casadei, P. Nielsen, G. Serra, A. Tani, “Evaluation of the input current quality by three different modulation strategies for SVM controlled matrix converters with input voltage unbalance”, Proceedings of IEEE/PEDES ‘96, Vol. II, New Delhi, 8-11 Jan. 1996, pp. 794-800.

[18] D. Casadei, G. Serra, A. Tani, “Reduction of the input current harmonic content in matrix converter under input/output unbalance”, IEEE Transactions on Industrial Electronics, Vol. 45, N. 3, June 1998, pp. 401-411.

[19] D. Casadei, G. Serra, A.Tani, “A general approach for the analysis of the input power quality in matrix converters”, IEEE Transactions on Power Electronics, Vol. 13, N. 5, September 1998, pp. 882-891.

[20] T. Matsuo, S. Bernet, R.S. Colby and T.A. Lipo, “Application of the Matrix Converter to Induction Motor Drives,” Conference Record of the Thirty-First IEEE/IAS Annual Meeting, 1996, Volume: 1, pp. 60-67, 1996.

[21] S. Bernet, T. Matsuo and T.A. Lipo, “A Matrix Converter Using Reverse Blocking NPT-IGBT’s and Optimised Pulse Patterns,” Proceedings of IEEE/PESC’96 , Baveno, Italy, June 1996, pp. 107-113.

[22] P. Nielsen, F. Blaabjerg, J.K. Pedersen, ”Space vector modulated matrix converter with minimised number of switchings and feedforward compensation of input voltage unbalance,” Proceedings of IEEE/PEDES’96, vol. 2, pp. 833-839, 1996.

[23] P. Nielsen, “The matrix converter for an induction motor drive,” Industrial Ph.D. project EF493, ISBN 87-89179-14-5, 296 pages, Aalborg University, Denmark,1996.

[24] D. Casadei, G. Serra, A. Tani, P. Nielsen, “Theoretical and experimental analysis of SVM-controlled matrix converters under unbalanced supply conditions,” Electromotion Journal, vol. 4, n° 1-2, pp. 28-37, 1997.

[25] F. Blaabjerg, D. Casadei, C. Klumpner, M. Matteini, “Comparison of two current modulation strategies for matrix converters under unbalanced input voltage conditions,” Proceedings of ISIE 2000, International Symposium on Industrial Electronics, December 4-8 2000, Puebla, Mexico, Vol. 2, pp. 465-470.

[26] D. Casadei, C. Klumpner, M. Matteini, G. Serra, A. Tani, “Input power quality in matrix converters: minimization of the RMS value of input current disturbances under unbalanced and nonsinusoidal supply voltages,” Proceedings of IEEE/NORPIE/2000, pp. 129-133, 2000.